AMOC Trends From 1850 to 2100 At Interannual To Multi-Decadal Time Scales Corroborated By Changes In Salinity Budget

Delphine Lobelle (d.m.a.lobelle@uu.nl)
Utrecht University https://orcid.org/0000-0003-1517-4815
Florian Sévellec
Laboratoire d'Oceanographie Physique et Spatiale, Univ. Brest,
Claudie Beaulieu
University of California
Valerie Livina
National Physical Laboratory
Eleanor Frajka-Williams
University of Southampton Waterfront Campus

Research Article

Keywords: AMOC, Slowdown likelihood, Intrinsic and forced variability, Climate change

Posted Date: January 11th, 2022

DOI: https://doi.org/10.21203/rs.3.rs-1231837/v1

AMOC trends from 1850 to 2100 at interannual to multi-decadal time scales corroborated by changes in salinity budget

Delphine Lobelle · Florian Sévellec · Claudie Beaulieu · Valerie Livina · Eleanor Frajka-Williams

Received: date / Accepted: date

Abstract The Atlantic Meridional Overturning Circulation (AMOC) is a key player in the global coupled ocean-atmosphere climate system. To characterise the potential of an AMOC slowdown, a past and future trend probability analysis is applied using 16 models from the Coupled Model Intercomparison Project Phase 5. We determine the probability of AMOC annual to multidecadal trends under the historical period and two future climate scenarios ('business-as-usual' scenario – RCP8.5 and 'stabilisation' scenario – RCP4.5). We show that the probability of a AMOC decline in model data shifts outside its range of intrinsic variability (determined from the pre-industrial control runs) for sustained 5-year trend or longer. This suggests that interannual AMOC events are not significantly affected by future climate scenario, and so potentially neither by anthropogenic forcing. Furthermore, under the 'business-as-usual' scenario the probability of a 20-year decline remains high (87%) until 2100, however in a 'stabilisation' scenario the trend probability recovers its pre-industrial values by 2100. A 20-year unique event is identified from 1995 to 2015, marked by simultaneous unique features in the AMOC and salinity transport that are not replicated over any other 20-year period within the 250 years studied. These features include the maximum probability and magnitude of an 'intense' AMOC decline, and a sustained 20-year decline in subpolar salinity transport caused by internal oceanic processes (as opposed to external atmospheric forcing). This work therefore highlights the potential use of direct salinity transport observations, and ensemble mean numerical models to represent and understand changes in past, present, and future AMOC.

Keywords AMOC · Slowdown likelihood · Intrinsic and forced variability · Climate change

D. Lobelle
Ocean and Earth Science, University of Southampton, Southampton, United Kingdom
Data Science Department, National Physical Laboratory, Hampton Road, Teddington, UK
Tel.: +31651921743
E-mail: d.m.a.lobelle@uu.nl
Present address:Institute for Marine and Atmospheric Research, Utrecht University, Utrecht, Netherlands

F. Sévellec
Ocean and Earth Science, University of Southampton, Southampton, United Kingdom
Present address:Laboratoire d'Océanographie Physique et Spatiale, Univ. Brest, CNRS, IRD, Ifremer, Brest, France

C. Beaulieu
Ocean and Earth Science, University of Southampton, Southampton, United Kingdom
Present address:Ocean Sciences Department, University of California, Santa Cruz, CA, USA

V. Livina
Data Science Department, National Physical Laboratory, Hampton Road, Teddington, UK

E. Frajka-Williams
National Oceanography Centre, University of Southampton Waterfront Campus, European Way, Southampton, SO14 3ZH, UK

1 Introduction

The AMOC redistributes heat, salt and carbon in the ocean (Ganachaud and Wunsch, 2003). In the present climate, the upper limb of the AMOC transports warm and salty waters northwards, where they release heat to the atmosphere in the northeast North Atlantic (Hall and Bryden, 1982), impacting European and global climate (Pohlmann et al, 2006). This sustained northward flux of salt and release of heat in the subpolar North Atlantic contributes to the formation of dense waters through deep convection (Manabe and Stouffer, 1988). The relationship between the AMOC and temperature and salinity fluxes in the North Atlantic contribute to feedback loops in the large-scale ocean overturning (Marotzke, 1996) which can be disrupted in potential future scenarios where the AMOC transport slows significantly. This study aims to (i) determine whether there are any periods of a higher probability of a decline in the AMOC transport from 1850 to 2100 (i.e., during the historical period and future climate projections), and (ii) identify whether salinity transports active in atmospheric and oceanic feedbacks are associated with the probability of a decline.

From AMOC observations using data from the RAPID array, Moat et al (2020) suggest that from 2004 to 2008 the AMOC had a constant mean transport followed by a step change and a lower constant mean from 2008 to 2018. A longer-term (centennial) forced signal can potentially exhibit shorter (decadal) periods of intrinsic variability, with an opposing (or absent) trend (Easterling and Wehner, 2009). For example, this can be seen in historical atmospheric temperature data where the multi-decadal trend experiences a hiatus or stabilisation period (Sévellec et al, 2016). Hence, our aim is also to verify whether the decadal decline reported from the RAPID AMOC observations can be a consequence of intrinsic variability or is part of a longer-term trend forced by climate change.

Other studies have turned to proxies to assess the multi-decadal past characteristics of the AMOC. Most conclude that over the last 50-100 years, the AMOC has probably not experienced an anthropogenically-driven decline, and trends from natural variability have been weak (Buckley and Marshall, 2016). Parker and Ollier (2016) use a combined observational proxy since 1860 to show that trends fall within the range of interannual to multi-decadal variability of the AMOC. Numerical hindcast simulations also support that the increase seen from the 1980s to mid-1990s, and a decline thereafter, are indicative of the quasi-decadal (to quasi 30-year) intrinsic AMOC variability (Huang et al, 2012a,b; Robson et al, 2014) and Worthington et al (2021) use deep-sea transport to build a 30-year reconstruction of the AMOC that shows no trend. On the other hand, Rahmstorf et al (2015) uses another proxy to show that a 20-year weakening from 1975 to 1995 was unprecedented and had a <0.005 probability of occurring due to natural variability alone. Furthermore, Caesar et al (2021) also suggest that the state of the AMOC is currently at its weakest in the last few decades. Such inconsistencies regarding the intrinsic or extrinsic forces of AMOC changes are explored in a coupled model-mean probability analysis here.

Future projections from the IPCC Fifth Assessment Report and follow-up studies have focused on the likelihood of a centennial decline by 2099 (Stocker et al, 2013; Schleussner et al, 2014). A reduction in AMOC strength is likely (within the 66%-percentile) by the end of the 21st century. Studies do, however, show a wide model spread of 12-30% likelihood in a climate stabilisation scenario (RCP4.5) and 25-56% likelihood in the 'business-as-usual' (RCP8.5) scenario (Weaver et al, 2012; Schleussner et al, 2014). Declining trend intensities also have a broad range, from 0 to 0.9 Sv per decade under the RCP8.5 scenario (Roberts et al, 2014; Smeed et al, 2018). Likelihood of declines on different timescales is still under discussion, however, hence the current study's focus.

To understand changes in the likelihood of an AMOC decline, one can focus on changes in North Atlantic transport dynamics, namely distinguishing overturning and horizontal gyre transport of temperature and salt. A positive feedback in ocean salinity transport was first described (in the context of estuary dynamics, though) by Stommel (1961), where a reduction in the AMOC volume transport results in less salt reaching the North Atlantic, thereby reducing the density of northern surface waters, weakening deep convection and thus weakening the AMOC (Marotzke, 1996). It means that an initial perturbation towards a weaker AMOC can be self-sustaining, leading to further or continued weak AMOC transport. The AMOC's sensitivity to freshening thresholds (or bifurcation points) can force the AMOC into a stable reduced or collapsed state (Stommel, 1961; Manabe and Stouffer,

1988; Rahmstorf, 2000; Dijkstra, 2007; Sévellec and Fedorov, 2011). Evidence for a possible bi-stability of the AMOC (where the AMOC has a stable 'on' and a stable 'off' state) has been seen in the geological record, suggesting that deep water formation can 'switch off' during abrupt climate shifts. It has been hypothesised that the switch is initiated by freshwater discharge in the northern North Atlantic (Broecker et al, 1985; Dansgaard et al, 1993; Broecker, 1998; Bond et al, 1999). Since then, global numerical models have been used to diagnose an AMOC shutdown threshold, and its early warning signals, by simulating an increase in atmospheric carbon dioxide (and hence an increase in surface temperature), or anomalously strong freshwater input in the subpolar North Atlantic, also called "hosing" experiments (Manabe and Stouffer, 1994; Rahmstorf, 1995; Wood et al, 1999; Zhang and Delworth, 2005; Stouffer et al, 2006; Boulton et al, 2014). From the CMIP5 ensemble, however, none show a likelihood of a total collapse within the 21st century as a consequence of global warming (Gregory et al, 2005; Weaver et al, 2012).

Other numerical model studies have focused on simulating potential North Atlantic temperature and salinity changes in the nearer future and examining the AMOC's response. An example includes the effects of anthropogenic warming on freshwater flux by Greenland ice sheet melting (Bakker et al, 2016) and Arctic ice retreat (Sévellec et al, 2017), both of which are not well represented in CMIP5 models (Stocker et al, 2013). Thorpe et al (2001) show that with a 2% increase in CO_2 per year over 70 years, a 20% weakening of the AMOC occurs, of which 60% is attributed to an increase in temperature at high latitudes and 40% to salinity decreasing at high latitudes and increasing at lower latitudes. Similarly, Hu et al (2009) show that a 1% per year increase of Greenland freshwater melt flux induces a 26% AMOC reduction in the last 20 years of the 21st century relative to the 20th century. Other studies, however, did not find a weakening AMOC with a forced increase in CO_2 (Latif et al, 2000) or found that freshwater anomalies have not yet impacted the AMOC (Böning et al, 2016). These results demonstrate the wide spread in AMOC behaviour in different models (Schmittner et al, 2005; Manabe and Stouffer, 1999). Due to large uncertainty in the response to forcing when using one model, we have are using a multi-model ensemble.

To explore the recent past changes, observations using hydrographic data from the Labrador Sea and six cruises across 24.5°N have shown that since the 1960s, a sustained freshening of the North Atlantic has occurred (Dickson et al, 2002; Hall and Bryden, 1982; McDonagh et al, 2015). This has played an important role in producing record low densities by 2015 (Robson et al, 2016). Though the cause is still under discussion, one possibility is a change in atmospheric forcing via a recent increase in precipitation over the subpolar gyre (Josey and Marsh, 2005). McDonagh et al (2015) on the other hand, focus on the respective contribution of the overturning or gyre transports in freshwater divergence between the Bering Strait and 26.5°N. They show that the positive freshwater flux (of 0.37 Sv) is dominated by the AMOC, which explains 91% of the variance, while the horizontal gyre component has a much smaller impact. Separating the circulation components (into overturning and horizontal gyre) can help to elucidate drivers of a flux change, and is therefore used in this study.

We have organised the paper into two parts. We first look at the probability and intensity of a past or future decline in the AMOC using over two centuries of data in coupled numerical models. We quantify the magnitude of trends of different durations to aid in understanding the modelled AMOC's interannual to multi-decadal properties through time. We then generate salinity budgets in the North Atlantic subtropical and subpolar gyres to examine the changes in differences and fluxes between these regions from 1850 to 2099. The motivation for this latter part is to investigate the role of changes to salinity feedback loops in increasing the probability and intensity of an AMOC decline.

2 Data

This study uses a selection of 16 CMIP5 models, namely: (1) ACCESS1-0, (2) bcc-csm1-1, (3) BNU-ESM, (4) CanESM2, (5) CCSM4, (6) CESM1-BGC, (7) CMCC-CM, (8) CNRM-CM5, (9) CSIRO-Mk3-6-0, (10) EC-EARTH, (11) GISS-E2-R-CC, (12) HadGEM2-CC, (13) IPSL-CM5A-MR, (14) MPI-ESM-LR, (15) MRI-CGCM3, (16) NorESM1-M. Four datasets are used: (i) control simulations, which are based on pre-industrial atmospheric

greenhouse gas emissions, (ii) historical simulations, which are based on post-industrial forcing from 1850 to 2005, (iii) the RCP4.5 future 'stabilisation' of emissions scenario, and (iv) RCP8.5 future 'business-as-usual' scenario; the latter two are from 2006 to 2099. The vertically- and zonally-integrated AMOC transport streamfunction is taken at 48°N and at a depth of 1,000 m. This latitude is chosen since the salinity transports (in the subpolar and subtropical regions) show a different behaviour north and south of 48°N (further explained in the Results section). The original data are monthly and we remove the seasonal cycle by subtracting each month's overall means before estimating trends for each dataset separately; the control, historical, RCP4.5 and RCP8.5.

The salinity [psu] and absolute potential temperature [K] profiles that vary in time and 3D space are extracted from the same 16 models and annual means are computed from monthly-mean data, only from the historical and RCP8.5 scenario output data this time. The number of vertical levels among the 16 models vary from 31 to 70, with a resolution ranging from 4.5 m to 15 m at the surface, and 206 m to 550 m at the bottom. The North Atlantic data are extracted between 96°W and 2°W (from the Gulf of Mexico, inclusive, to the eastern African coast) and 20°N to 60°N. The models are first re-gridded to a $2^\circ \times 2^\circ$ resolution by finding the nearest neighbour longitude and latitude using even values. Though this re-gridding could introduce some degree of uncertainty regarding mass preservation, it is required to compare the models and acquire an ensemble mean as a function of latitude, since their original grids have different horizontal resolutions. The North Atlantic is then split into two regions, the subtropical region (STR) and the subpolar region (SPR). As described above for the AMOC, the boundary between the STR and SPR is determined robustly at 48°N.

3 Methods

3.1 Interannual to multi-decadal AMOC trends

The CMIP5 pre-industrial control simulations are used to represent what will hereafter be referred to as 'intrinsic variability' of the AMOC, hence, variability existing in the absence of 'external forcing', such as anthropogenic greenhouse emissions, volcanic eruptions, and solar activity changes. Moving linear regression trends are fit to each of the 16 models' control timeseries using sliding windows of 2, 10, 20, and 40 years (and sliding in increments of 12 months). The trend magnitudes of all the sliding windows are placed into 50 equally-spaced bins to generate a probability density function (PDF) for each of the 16 models. These 16 PDFs are averaged in order to generate the multi-model ensemble mean reference PDF that defines the intrinsic variability of the AMOC in this study. This ensemble mean PDF is therefore centred around zero, where positive values indicate an increasing AMOC trend and negative values a decreasing trend. Following the assumption stated in the design of the IPCC's future scenarios that no drastic changes in natural variability occur (which includes both intrinsic variability and variability forced by natural effects, such as volcanic eruptions or changes in solar forcing, Stocker et al, 2013) we also assume that intrinsic variability stays constant through time. This results in four reference PDFs: one for each of the sliding window trend lengths (hereafter referred to as 2, 10, 20 and 40-year trend durations).

The 'forced' component can now be computed relative to the 'intrinsic variability' that has been defined. It is estimated here by the ensemble mean trends from three timeseries: (i) CMIP5 historical scenario (1850–2005), (ii) future RCP4.5 (2006–2099) and (iii) future RCP8.5 (2006–2099). As opposed to the intrinsic variability that we assume to be constant through time, here we assess the effects of the forcing using both the time-averaged trends and time-varying trends. The forced trend is computed as the model-mean trend of the 16-model-ensemble simulations. The same sliding window technique as stated above is used over the 250 years (historical followed by RCP4.5 and historical followed by RCP8.5). For the time-averaged analysis, trends of the four trend durations from 1850 to 2005 are averaged to represent the historical mean trends and from 2006 to 2100 for both RCP4.5 and RCP8.5 to represent the two future scenarios' trends. That one value, representing the time-averaged ensemble mean (forced) trends, is summed to each of its respective intrinsic variability (control) PDFs described in the previous paragraph. A hypothetical illustration of this is shown (in Figure S1). A reference PDF (Figure S1a) that

experiences a time-averaged forced increase in AMOC strength would shift the entire PDF to the higher positive AMOC trend values (Figure S1b), leading to a higher probability of an AMOC increase; on the other hand a time-averaged forced decline in AMOC strength would shift the entire PDF to the higher negative trend values (Figure S1c), leading to a higher probability of an AMOC decrease. For the time-varying part of the analysis, the reference PDF shifts to positive or negative values depending on the forced trend, however this time the trend is computed at each time step from 1850 to 2100. Once again, this is repeated for the same four reference PDFs (for the four trend durations) and for the historical followed by RCP4.5 and historical followed RCP8.5 timeseries.

Elaborating on the method in Sévellec et al (2016), the full range of trend magnitudes found in the reference PDF is split into six probability categories (see Figure S1 and Equations 1): (1) intense decrease ($P_{\searrow int}$ in Equation 1a), (2) moderate decrease ($P_{\searrow mod}$ in Equation 1b), (3) weak decrease ($P_{\searrow weak}$ in Equation 1c), (4) weak increase ($P_{\nearrow weak}$ in Equation 1d), (5) moderate increase ($P_{\nearrow mod}$ in Equation 1e), and (6) intense increase ($P_{\nearrow int}$ in Equation 1f). These categories are based on the probability of trends in the multi-model control PDF falling below 1 standard deviation ('weak'), from 1 to 2 standard deviations ('moderate'), and above 2 standard deviations ('intense'). These probability categories read:

$$P_{\searrow int} = P(\beta \leq -2\sigma) = \int_{-\infty}^{-2\sigma} p(\beta)\, d\beta, \tag{1a}$$

$$P_{\searrow mod} = P(-2\sigma < \beta \leq -\sigma) = \int_{-2\sigma}^{-\sigma} p(\beta)\, d\beta, \tag{1b}$$

$$P_{\searrow weak} = P(-\sigma < \beta \leq 0) = \int_{-\sigma}^{0} p(\beta)\, d\beta, \tag{1c}$$

$$P_{\nearrow weak} = P(0 < \beta \leq +\sigma) = \int_{0}^{+\sigma} p(\beta)\, d\beta, \tag{1d}$$

$$P_{\nearrow mod} = P(+\sigma < \beta \leq +2\sigma) = \int_{+\sigma}^{+2\sigma} p(\beta)\, d\beta, \tag{1e}$$

$$P_{\nearrow int} = P(+2\sigma < \beta) = \int_{+2\sigma}^{+\infty} p(\beta)\, d\beta, \tag{1f}$$

where σ is the standard deviation of the intrinsic variability (i.e., from the multimodel average reference PDF), β is the forced trend (i.e., from the historical or future scenario data), and p is the probability density function. We can also define the probabilities of increase and decrease as: $P_{\nearrow}$=$P_{\nearrow weak}$+$P_{\nearrow mod}$+$P_{\nearrow int}$ and $P_{\searrow}$=$P_{\searrow weak}$+$P_{\searrow mod}$+$P_{\searrow int}$, respectively. The $p(\beta)$ here can either be the probability density function of the time-averaged trends, or the time-varying trends. The six computations of Equation 1, are repeated for each of the moving-window trend filters (2, 10, 20, and 40 years), and for each forced scenario (historical, RCP4.5 and RCP8.5). This determines the probability of the six categories for interannual to multi-decadal trends in each scenario.

Lastly, the expected intensity of both an increasing and decreasing trend is computed. As opposed to the six probability categories above (in Equation 1), there are now only two categories, the expected decrease ($E_{\searrow}$), and the expected increase ($E_{\nearrow}$), which are estimated as follows:

$$E_{\searrow} = \frac{\int_{-\infty}^{0} p(\beta)\,\beta d\beta}{\int_{-\infty}^{0} p(\beta)\,d\beta}, \tag{2a}$$

$$E_{\nearrow} = \frac{\int_{0}^{+\infty} p(\beta)\,\beta d\beta}{\int_{0}^{+\infty} p(\beta)\,d\beta}, \tag{2b}$$

where now we only compute the probability density function, $p(\beta)$, for the time-varying trends, and not time-averaged. Therefore, the $E_{\searrow}$ and $E_{\nearrow}$ are time-varying expected intensities of an AMOC negative trend and positive trend, respectively. It is important to note that though this analysis uses the AMOC at 48°N, it was also performed for 20 to 60°N (not shown), and produced similar results. Therefore, comparisons with previous work using other latitudes (for example, 26.5°N) are valid.

3.2 Estimating the North Atlantic salinity budget

The mathematical framework used to estimate the North Atlantic salinity budget in this study has been used in several studies focusing on meridional temperature or salinity fluxes (Bryden et al, 2011; Drijfhout et al, 2011; Weaver et al, 2012; McDonagh et al, 2015; Mecking et al, 2016, 2017). It was formulated by Rahmstorf (1996) and de Vries and Weber (2005), where a rigorous derivation can be found in Mecking et al (2016), and it is derived in further detail in the supplementary information.

Oceanic salinity transports are expressed here as an overturning component ($\mathscr{S}_{\mathrm{ov}}$) and an azonal component, from the gyre recirculation ($\mathscr{S}_{\mathrm{az}}$). Following results from Mecking et al (2016), the atmospheric forcing salinity flux (via precipitation and evaporation with the addition of the runoff) is assumed to dominate the residual term ($\mathscr{F}$), so the distinction between internal oceanic ($\mathscr{S}_{\mathrm{ov}}$ plus $\mathscr{S}_{\mathrm{az}}$) and external atmospheric ($\mathscr{F}$) transport can be made. Hence, the sum of the divergence of $\mathscr{S}_{\mathrm{ov}}$ and $\mathscr{S}_{\mathrm{az}}$ minus the time derivative of total net salinity transport in a region is used to estimate the external atmospheric salinity forcing term (i.e., the residual). Changes to these individual components, as well as the overall salinity transport in the STR and SPR, are used to identify whether the AMOC slowdown is primarily driven by the external atmospheric processes or internal ocean processes. The derivations of these terms are now described below.

As mentioned above, two regions are used in our model, the subtropical 'box' from 20–48° N and the subpolar 'box' from 48–60° N. To estimate the salinity budget between these boxes, we use the advective-diffusive equation. We set box boundaries, allowing for free flow into and out of the boxes only via their northern and southern edges and the sea-surface to atmosphere. Using the subpolar box as an example, the time derivative of salinity transport is computed as the difference between the southern and northern boundary meridional transport plus a residual:

$$\int_X \int_Y \int_Z \partial_t S\,dx\,dy\,dz = \int_X \int_Z (vS)|_{y=48^\circ\mathrm{N}}\,dx\,dz - \int_X \int_Z (vS)|_{y=60^\circ\mathrm{N}}\,dx\,dz + \mathscr{F}. \tag{3}$$

where $\int_X$ is the zonal integral, $\int_Y$ is the meridional integral and $\int_Z$ is the vertical integral, S is salinity, v is meridional velocity and F is the residual flux. Although the residual can consist of a few components (see Eq. 8 in SI) we assume that the surface boundary flux (forcing term) dominates. This follows results from Mecking et al (2016),

that evaporation-precipitation+runoff is almost an order of magnitude larger than the other diffusive mixing or eddy terms in the North Atlantic subpolar and subtropical regions in this set of CMIP5 experiments.

Salinity and meridional velocity can be split into their respective zonal means and anomalies $(\overline{v}+v')$ and $(\overline{S}+S')$. The average terms are then separated into two terms: (i) the zonally and vertically averaged net term (or 'net', a constant along the zonal and vertical direction), and (ii) the overturning component (or 'ov', that varies only vertically; a constant along the zonal direction). An anomaly remains as one term which is azonal (or 'az', that varies zonally and vertically). Hence this decomposition reads:

$$\mathscr{S} = \int_X \int_Z (v_{\text{net}} + v_{\text{ov}} + v_{\text{az}})(S_{\text{net}} + S_{\text{ov}} + S_{\text{az}})\, dx\, dz. \tag{4}$$

The components of the flow in terms of overturning and azonal flows, the transport of salinity at a given latitude reads:

$$\mathscr{S}_{\text{ov}} = \int_Z \mathscr{W}_x v_{\text{ov}} S_{\text{ov}}\, dz, \tag{5a}$$

and

$$\mathscr{S}_{\text{az}} = \int_X \int_Z v_{\text{az}} S_{\text{az}}\, dx\, dz, \tag{5b}$$

where $\mathscr{W}_x$ is the full width of the Atlantic basin. The $\mathscr{S}_{\text{ov}}$ and $\mathscr{S}_{\text{az}}$ is computed at three latitudes (20°N, 48°N and 60°N) to estimate the salinity transport across the northern and southern boundaries of the subpolar and subtropical boxes. To close the budget, the time derivative of integrated salinity in the each box becomes the sum of three components: the difference between the $\mathscr{S}_{\text{ov}}$ at the northern and southern boundaries of the box plus the difference between the $\mathscr{S}_{\text{az}}$ at the same latitudes, plus the total residual term. Using the subpolar box (SP) as an example we have:

$$\begin{aligned} &\int_X \int_Y \int_Z \partial_t S|_{\text{SP}}\, dx\, dy\, dz \\ &= (\mathscr{S}_{\text{ov}}|_{48^\circ\text{N}} - \mathscr{S}_{\text{ov}}|_{60^\circ\text{N}}) + (\mathscr{S}_{\text{az}}|_{48^\circ\text{N}} - \mathscr{S}_{\text{az}}|_{60^\circ\text{N}}) + \mathscr{R}_{\text{total}} = \Delta\mathscr{S}_{\text{ov}}|_{\text{SP}} + \Delta\mathscr{S}_{\text{az}}|_{\text{SP}} + \mathscr{F}|_{\text{SP}}. \end{aligned} \tag{6}$$

To compare anomalies of each component, we define a reference year which is defined in this study as the year when the accumulated transport is zero (t_{ref} = 1975); note that our results therefore depend on this reference year definition. By removing the mean over the beginning of the timeseries to t_{ref} (from t_0=1851 to 1975), this allows all fluctuations in the timeseries until 1975 to oscillate around zero, after which the future accumulated anomalies are more easily distinguishable (over 1975 to 2099). Using one of the components, $\mathscr{S}_{\text{ov}}$, at any latitude as an example, the anomaly of $\mathscr{S}_{\text{ov}}$ is:

$$\mathscr{S}_{\text{ov}}|_{\text{anom}}(t) = \mathscr{S}_{\text{ov}}(t) - \frac{1}{t_{\text{ref}}} \int_{t_0}^{t_{\text{ref}}} \mathscr{S}_{\text{ov}}(t')\, dt'. \tag{7}$$

The accumulated anomaly transport of the overturning component (which therefore recovers a measure of salinity content) then reads:

$$\Sigma_{\text{ov}}(t) = \int_{t_0}^{t} \mathscr{S}_{\text{ov}}|_{\text{anom}}(t')\, dt', \tag{8}$$

where Σ is the accumulated anomaly of any transport and $\Sigma(t_{\text{ref}})$ = 0 by definition. Smoothing of the accumulated annual data is then performed using a 10-year moving-average.

Finally, a direct comparison to the 20-year forced moving trends of the AMOC transport is done, where linear regressions of 20-year sliding windows for each salinity transport component from 1851 to 2099 are computed and represented as $\Theta\mathscr{S}$. The 20-year window slides in increments of one year, to produce a timeseries as a function of the midpoint of this window.

The mathematical derivations of the salinity budget above can provide insight regarding the components driving the salinity feedback loop associated with the AMOC. Under certain conditions (such as anthropogenic forcing), the AMOC could respond to thresholds due to positive feedbacks (Stommel, 1961). A key driver of the posi-

tive oceanic feedback that destabilises the AMOC is anomalous freshwater input in the subpolar North Atlantic (Stommel, 1961; Baumgartner and Reichel, 1975). If the AMOC weakens (regardless of the original cause), the near-surface waters that carry heat and salt to the deepwater formation sites also slow down. At high latitudes, since it is a region of net freshwater input from the atmosphere, transit time of AMOC surface waters passing through is increased, therefore further decreasing the rate of poleward salt transport. This reduces the salinity of the water and hence the density, which further weakens the overturning via this positive feedback (Urban and Keller, 2010; Marotzke, 1996).

4 Results and discussion

4.1 AMOC trends

This study uses the control ensemble PDFs as a reference, representing the AMOC's intrinsic variability, where trend values range from -3 to $+3$ Sv yr^{-1} across the 16 models for the 2-year trends (Figure 1a) and -0.1 to $+0.1$ Sv yr^{-1} for the 40-year trends (Figure 1d). These PDFs show an almost symmetrical probability (also known as zero skewness) of an increase or a decrease in the AMOC transport, regardless of the trend length (Figure 1a, b, c, and d). The interannual, decadal, and multi-decadal forced trends in historical and 21st century (RCP4.5 and RCP8.5) scenarios are now considered (Figures 5 and 6), both as time-mean and time-varying forcing, in order to discuss the total (intrinsic plus forced) variability from 1850 to 2099. The timing of a shift in probabilities is revealed when considering these PDFs as a function of time, among the combined ensemble historical and future scenario data (Figure 3 and 4).

4.1.1 Historical interannual to multi-decadal trends

The historical ensemble PDFs are almost identical to the controls', meaning that the average interannual to multi-decadal forced trends of the AMOC from 1850 to 2005 are equivalent to intrinsic variability (Figure 1a, b, c, and d). The forcing, on average, is therefore negligible over the historical period. The time-varying trends, however, show that there are large oscillations around zero (Figures 5 and 6), which produce time-evolving shifts in the probability of a weak increase ($P_{\nearrow \text{weak}}$) or a weak decrease ($P_{\searrow \text{weak}}$) in the AMOC (Figures 3 and 4). This demonstrates that the effects of forcing on probabilities of strengthening and weakening are time-dependent. Although, these variations of the probabilities are attributed to the forcing, by construction of the PDFs, in reality observations come from a single realisation from such a PDF. Hence the relative contributions of intrinsic and forced signals on the trends cannot be easily distinguished in observations (or in single model realisation). A study using one iteration of an AMOC timeseries (an observational proxy) recovers a stable AMOC since 1860, without finding any trends that fall outside the range of interannual to multidecadal intrinsic variability (Parker and Ollier, 2016). On the other hand, Rahmstorf et al (2015) suggest that the 20-year decline from 1975 to 1995 had almost a 100% probability of being anthropogenically-caused. Here, the results indicate that when using a timeseries constructed from an ensemble mean of forced historical AMOC trends from 1850 to 2005, the time-average is dominated by intrinsic variability.

4.1.2 Interannual (two-year) trends in the 21$^{\text{st}}$ century

The future scenario interannual PDFs (2-year time-mean trends in Figure 2 and 1a) mirror the control and historical PDFs. The time-varying trends and probabilities (Figures 5a and 6a, and Figures 3a and 4a) also represent a similar behaviour to the historical period. This illustrates that even though the AMOC is under two climate change scenarios, on higher-frequency timescales, the time-mean and time-varying intrinsic variability is larger than the forced changes (the signal-to-noise ratio is weak). An example of the implications of these findings is that the probability of an event such as the potential decline observed over 14 months between 2009-2010 (corresponding

to a 30% decrease, McCarthy et al, 2012; Srokosz et al, 2012; Bryden et al, 2014), falls within the range of intrinsic variability. Ezer (2015) suggests that this so-called 'extreme event' is the last part of a longer, decadal trend, that started before RAPID (according to three observational datasets from 2000). It is worth noting that McCarthy et al (2012) and Roberts et al (2014) suggest that the CMIP5 ensemble underestimates the observed interannual variability and trends (of the 2009-2010 magnitude, 4.7 Sv, for example), though. However this ratio between the trends and the variability could still be accurate, therefore not affecting our conclusions.

4.1.3 Five-year and decadal trends in the 21st century

Upon examining five-year and 10-year trends in the 21st century, the average probability of seeing a decline in the future scenarios increases slightly, shown by a small shift in the PDFs towards negative values (Figure 1b). The average probability of a weak decline from 2006-2099 for 10-year trends is 61.3% and 67.1% under an RCP4.5 and RCP8.5 scenario, respectively (Figure 1b and 2). The time-varying forced trend intensities are generally negative throughout the 21st century in both scenarios (Figures 5b and 6b), although the last few decades under RCP4.5 show a recovery of the forced trends oscillating around zero. The historical time-varying $P_{\nearrow}$ and $P_{\searrow}$ remains well balanced, with one moderate $P_{\searrow}$ peak at the turn of the century in both RCP4.5 and RCP8.5 (Figures 3b and 4b), and RCP4.5 again returns to probabilities oscillating between a $P_{\nearrow}$ and $P_{\searrow}$ by 2099. Contrary to the interannual results, since a forced decadal decline is probable at the turn of the century (of 79% in 2010 for 'business-as-usual'), the observed decadal trend from RAPID of -0.41 (± 0.18) Sv yr^{-1} between 2004 and 2014 (Jackson et al, 2016) was likely to occur, according to the RCP4.5 and RCP8.5 ensemble mean forcing here. These results suggest that the AMOC variations therefore start being statistically impacted by forcing trends on durations longer than 5 years.

4.1.4 Inter-decadal (20-year) trends in the 21st century

The 20-year ensemble time-mean trends in the 21st century generate a distinctively augmented AMOC slow-down probability than when evaluated with shorter timescales. The average probabilities of a 20-year decline from 2006-2099 under an RCP4.5 and RCP8.5 scenario, are 72% and 87%, respectively (Figures 1c and 2). The most prominent feature is a rapid jump in both RCP4.5 and RCP8.5 20-year forced decline intensity (Figures 5c and 6c) and probability (Figures 3c and 4c) at the beginning of the 21st century, leading to a probability of a decline from 1995 to 2015 reaching 95% for both RCP4.5 and RCP8.5. This 20-year period, from 1995 to 2015 is therefore hereafter defined as the 'unique event', characterised by the maximum negative trend intensity and decline probability over the 250 years studied. The forced trend magnitude occurring over this unique event is -0.11 Sv yr^{-1} in both future scenarios (Figures 5c and 6c for RCP4.5 and RCP8.5, respectively). Pre-1995, the forced trends oscillate around zero and post-2015, the negative forced trends relax partially, under RCP8.5, and fully (back to zero), under RCP4.5. The time-varying probability of an intense 20-year decline ($P_{\searrow \mathrm{int}}$) reinforces the uniqueness of the unique event; it shows an intense decline probability of 50% under RCP4.5, and 56% under RCP8.5, compared to their pre-1995 maximum of 13% and post-2015 maxima of 24% and 38%, respectively (Figures 3c and 4c).

The timing of this 20-year unique event (1995-2015), for which we find an average probability of decline of 92% for RCP8.5 (and 91% for RCP45), is interestingly consistent with observational findings showing that the AMOC has indeed sustained a decline since the mid-1990s (Smeed et al, 2013; Robson et al, 2014). Robson et al (2016) associate the decline to a simultaneous dramatic decrease in the Labrador Sea density index, stimulated by a deep ocean warming and long-term freshening of the subpolar gyre waters. They mention that the exact contributors to this change in temperature and salinity remains an open question, and is therefore further investigated below. The results from this analysis suggest that 1995-2015 is a unique event where the AMOC is forced to decline, regardless of intrinsic variability.

4.1.5 Multi-decadal (40-year) trends in the 21st century

The 40-year time-mean ensemble trends produce the highest probabilities of an AMOC decline relative to the other trend durations (95% under RCP4.5, and 99% under RCP8.5 in Figures 1d and 2). The striking feature under the 'business-as-usual' scenario is the time-average probability of an intense decline ($P_{\searrow int}$) at 86%, whereas none of the other trend durations or scenarios exceed a $P_{\searrow int}$ of 50%. This is also seen in the time-varying RCP8.5 probabilities (Figure 4d), where there is a sustained high $P_{\searrow int}$ throughout the 21st century. This contrasts to the 20-year probabilities, where $P_{\searrow mod}$+$P_{\searrow int}$ oscillate around the 50% probability in the 21st century (Figure 4c). Because only negative trends are possible in RCP8.5, the time-varying intensity of the expected decline is identical to time-varying intensity of the forced trend (Figure S3d). Although the RCP4.5 probabilities also sustain a high $P_{\searrow int}$, after 2060, once again, the stabilisation of an equal probability of increase and decrease occurs by 2099 (Figure 3d), and expected trend intensity is no longer identical to ($E_{\searrow}$) (Figure S2d). Further smoothing of the trends (above 40 years) would mechanically increase the contribution of the forced trend over the intrinsic one, simply increasing the probability of a decline. Therefore, these results find that not only a multi-decadal but also a quasi-centennial sustained decline is highly probable throughout the 21st century (consistently with the IPCC report's conclusion in Weaver et al, 2012; Flato et al, 2013).

In summary, the first part of our results suggest that the AMOC's interannual intrinsic variability is stronger than the forced signal over 250 years, regardless of the forcing applied (future 'business-as-usual' or 'stabilisation'). The longer-term forced trends (more than five-years in duration) under future scenario anthropogenic forcing skew the probability to a decline. Both a 20-year unique event (from 1995 to 2015) and a sustained 21st century intense decline probability in RCP8.5 are seen. Under the RCP4.5 scenario, the balance between AMOC increase and decrease probability, equivalent to the historical and pre-industrial (control simulation) period, is recovered by the end of the 21st century for all tested trend durations. The next part of the analysis therefore investigates the cause of these probability changes, where the dynamical relationship between the AMOC and salinity fluxes can direct whether the changes originate from internal oceanic processes, or external atmospheric processes.

4.2 Analysis of the salinity budget

4.2.1 Salinity budget at equilibrium of the forced component

The 250-year forced timeseries of the various salinity transports (from 1851 to 2099) has been split into a reference period over the first 125 years (from 1851 to 1975) and a post-reference period over the following 125 years (1975 to 2099; Figure S6). The reference period presents fluxes that are almost in equilibrium when averaged temporally (with a small total residual of $+0.11$ Sv psu in the subtropical region (STR) and $+0.02$ Sv psu in the subpolar region (SPR; Figure 8). These reference salinity transports at the three latitudes used (20°N, 48°N, and 60°N), therefore represent the fluxes prior to the drift as part of climate change (Figure S6a).

All three latitudes have a positive, northwards flux of salt via both the overturning component and the horizontal gyre component, apart from $\mathscr{S}_{\rm az}|_{20^\circ{\rm N}}$ (southwards). This creates a divergence of salt by $\mathscr{S}_{\rm az}$ in the STR of almost equal transport northwards and southwards (-8.12 Sv psu via $\mathscr{S}_{\rm az}|_{20^\circ{\rm N}}$ and $+8.26$ Sv psu via $\mathscr{S}_{\rm az}|_{48N}$). $\mathscr{S}_{\rm ov}|_{20^\circ{\rm N}}$ induces the largest flux into the STR ($+15.58$ Sv psu) and $\mathscr{S}_{\rm ov}|_{60^\circ{\rm N}}$ the smallest flux out of the SPR ($+0.60$ Sv psu) (Figure 8). The generally northward fluxes are consistent with findings from Rahmstorf (1996) showing that freshwater transport from the overturning circulation is southwards everywhere in the North Atlantic (i.e., northwards salinity transport).

Upon examining the subtropical and subpolar regions' transports separately over the reference period, the combined positive and negative fluxes at different latitudes result in a net $\Delta\mathscr{S}_{\rm ov}$ import of salt into both the STR and SPR and a net $\Delta\mathscr{S}_{\rm az}$ export of salt out of both regions (Figure 7b and c). The highest salinity transport is via $\Delta\mathscr{S}_{\rm az}|_{\rm ST}$ export ($+16.38$ Sv psu), due to the divergence mentioned above. The total oceanic transports

$\Delta\mathscr{S}_{\mathrm{ov}} + \Delta\mathscr{S}_{\mathrm{az}}|_{\mathrm{ST}}$ and $\Delta\mathscr{S}_{\mathrm{ov}} + \Delta\mathscr{S}_{\mathrm{az}}|_{\mathrm{SP}}$ generate a transport of salt out of the STR (-7.38 Sv psu) and into the SPR ($+4.54$ Sv psu) during the reference period. The atmospheric forcing ($\mathscr{F}$) is computed as the residual component flux and the time-derivative of salinity (that is minimal during this quasi-equilibrium phase of the forced component). Assuming that the residual is primarily due to precipitation and evaporation (and also potentially river run-off) implies that at equilibrium there is freshwater outflux from evaporation in the STR (increasing salinity by $+7.50$ Sv psu), and freshwater influx from precipitation in the SPR (decreasing salinity by $+4.52$ Sv psu in Figure 7b and c and Figure 8).

4.2.2 Multi-decadal temperature and salinity anomalies in the 21st century

Salinity anomalies of the ensemble mean referenced to 1975, as a function of latitude and averaged over different depth ranges, further support that during the reference period, the concentrations do not vary greatly (shown by the Hovmöller plots in Figures 9 and S2). This next subsection looks at the anomalies as 10-year running means, and the analysis focuses on the period from 1975 to 2095, where the subtropical and subpolar forced components of salinity show a dramatic change compared to the reference period.

Although temperature changes are not the focus of this study, a brief description is mentioned here, to acknowledge the shared thermal and haline contributions to changes in buoyancy under external forcings (Stommel, 1961; Marotzke, 1996; Thorpe et al, 2001; Sévellec and Fedorov, 2011). The forced-component of the temperature anomalies, post-1975 and throughout the 21st century, increase almost uniformly throughout the North Atlantic upper ocean (top 2,500 m), or when averaged over the full depth under both CMIP5 future scenarios (Figures 9a, b, and d and S2a, b, and d for RCP4.5 and RCP8.5, respectively). For the surface values, this is consistent with Delworth et al (2007) showing that multi-decadal sea surface temperature patterns in the North Atlantic produce anomalies with the same sign on a basin scale between the equator and 60° N. This homogeneous warming coincides with the projections of anthropogenically-forced global atmospheric temperature rise, insinuating that the residual surface flux could play a dominant role in upper ocean temperature changes, as opposed to oceanic fluxes (although a temperature budget to verify this is outside the scope of this study). It is worth noting that the warming is stronger in the SPR than in the STR at all depths, leading to a negative meridional temperature gradient. The negative temperature feedback mechanism indicates that an increase in the gradient between the STR and SPR would onset a stronger AMOC transport (Marotzke, 1996), contrary to what we observed in the simulations. Although there are studies showing that from 50 to 60°N there is a subpolar 'Warming Hole' (Drijfhout et al, 2012), the CMIP5 zonally-integrated upper ocean ensemble mean does not exhibit this anomaly (Figures 9a and b and Figures S2a and b), possibly since the global mean temperature signal must be removed in order to identify it. Averages from 2,500 m to the bottom, however, show a decrease in temperature in the SPR, but not in the STR which still indicates a warming (Figures 9c and S2c for RCP4.5 and RCP8.5, respectively). With subpolar upper ocean waters becoming more positively buoyant as a result of an increase in temperature, a potential reduction in deep water convection could occur at the higher latitudes, causing a larger difference in temperature between above and below 2,500-m depth. Anomalous spatial patterns are consistent across results under the RCP4.5 and RCP8.5 scenarios, with the 'business-as-usual' scenario showing stronger anomalies (reaching a full depth average maximum of $+1.19$ K and $+0.76$ K by 2095 under RCP4.5 and RCP8.5, respectively).

Salinity anomalies, on the other hand, show a dipole response to forcing in the 21st century, with a freshening in the SPR and a salinification in the STR. This potentially suggests that the positive salinity feedback mechanism is generated under a warming climate, and a weakened AMOC is linked to a stronger salinity gradient between the SPR and STR, which further weakens the AMOC transport (Marotzke, 1996). The other hypothesis would be an intensification of the atmospheric water cycle, with stronger evaporation in the STR and precipitation in the SPR, which is a hypothesis formulated as a consequence of anthropogenically-forced climate change (Stocker et al, 2013). This ensemble mean salinity anomaly is consistent across all depth ranges and under both future scenarios (Figures 9 and S2 for RCP8.5 and RCP4.5, respectively), although the average below 2,500 m does not show an

increase in salinity in the STR (Figures 9g and S2g). The integrated anomalies averaged over the full depth are used to define the latitude (48°N) that separates the two regions dynamically in this study (Figures 9h and S2h). In the rest of this section the salinity budget, previously defined, is used to attribute the cause of the forced-component of the salinity change to either internal oceanic processes (i.e., positive salinity feedback through AMOC and gyre circulation change) or external atmospheric processes (i.e., intensification of the atmospheric water cycle).

By the end of the 21st century, the increase in the net STR salinity ($+0.09$ psu) and decrease in SPR salinity (-0.03 psu) relative to 1975 is seen, both as a function of latitude, averaged over the full water column (Figure 9h), and summarized from the salinity budgets (Figure 10). The accumulated anomalies since 1975 (Figure 11) of the oceanic salinity transports (Σ_{ov} and Σ_{az}) and atmospheric salinity flux ($\Sigma\mathscr{F}$) are used to address potential drivers of changes in long-term salinity transport over 125-year simulations.

At the three latitudes (20°N, 48°N, and 60°N), the transports generally tend towards an increase in salinity anomalies throughout the 21st century (Figure 11a). $\Sigma_{az}|_{20°N}$, $\Sigma_{ov}|_{60°N}$, and $\Sigma_{ov}|_{48°N}$ have slight negative anomalies for the first few decades before becoming positive by 2020, 2030, and 2060, respectively. The component with the largest total accumulated flux after 125 years is the $\Sigma_{az}|_{20°N}$ (with $+5.02$ Pm^3 psu), meaning it has drastically reduced its initial southward transport (compared to its reference fluxes in Figure 8), leading to retention of salt within the STR. $\Sigma_{az}|_{60°N}$ is also the dominant term for exporting salt in the SPR, reaching $+4.01$ Pm^3 psu by 2095 (Figure 10).

Combining the effects of the boundary fluxes provides an estimate of divergences and convergences of salinity within each region from 1975 to 2095. In the subtropics, the consistently positive exponential increase in accumulated salinity (Figure 11b) seems to be dominated by $\Sigma_{ov}|_{ST}$ until approximately 2050 (where it reaches its maximum of $+1.93$ Pm^3 psu). $\Sigma_{az}|_{ST}$ has an opposing effect, exporting salinity until 2060 (reaching its minimum in 2020 of -0.85 Pm^3 psu). Post-2060, joint efforts between the accumulated $\Sigma_{az}|_{ST}$ and increased evaporation ($\Sigma\mathscr{F}|_{ST}$) appear to dominate net accumulation of salinity ($\Sigma\mathscr{S}$), while $\Sigma_{ov}|_{ST}$ imports less salt until the end of the century (Figure 11b). Upon combining Σ_{ov} and Σ_{az}, the oceanic transports ($\Sigma_{ov+az}|_{ST}$) and atmospheric forcing ($\Sigma\mathscr{F}|_{ST}$) have almost identical exponentially increasing impact. This suggests that the forced salinity change in the subtropics comes evenly from oceanic internal dynamics and atmospheric external forcing.

The components of accumulated salt transport show large difference between STR and SPR dynamics. The largest difference between the SPR and STR dynamics is that the SPR's range of accumulated transports is a lot smaller than the STR's (between -1.45 and $+0.69$ Pm^3 psu in the SPR compared to -0.85 and $+3.54$ Pm^3 psu in the STR) (Figure 11b and c). Note that the first couple of decades (1975 to 2020) see an intriguing relationship between the components that is further investigated in Section 4.2.3 below. The general tendency after 2020 is an opposing effect between the atmospheric forcing ($\Sigma\mathscr{F}|_{SP}$), that causes a constant increase in salinity retention from 1975 to 2095 (implying a decrease in precipitation), and the oceanic transports ($\Sigma_{ov+az}|_{SP}$) that export more salinity. However, $\Sigma_{ov+az}|_{SP}$ dominates over the atmospheric term, leading to a net decrease in salinity in the SPR. Contrary to the STR, both Σ_{ov} and Σ_{az} in the SPR generally produce negative accumulated anomalies. (It is worth noting that in the subpolar region both overturning and azonal transport contribute to the AMOC, since the AMOC becomes a lot more horizontal than in the suptropical region).

These results indicate that by 2095, salinity change in the subtropics is equally due to oceanic feedback ($\Sigma_{ov+az}|_{ST}$) and atmospheric forcing ($\Sigma\mathscr{F}|_{ST}$), producing accumulated anomalies of $+3.70$ Pm^3 psu and $+3.54$ Pm^3 psu, respectively (Figure 10 and 11b). In the subpolar region, however, it is the ocean internal dynamics ($\Sigma_{ov+az}|_{SP}$) that dominate the salinity changes over the external atmospheric forcing ($\Sigma\mathscr{F}|_{SP}$), with values of -1.04 Pm^3 psu versus $+0.69$ Pm^3 psu, respectively (Figure 10 and 11c).

4.2.3 Unique 20-year AMOC event and its relation to salinity changes

We have identified a 'unique event' over 20-years (from 1995 to 2015) in which the AMOC at 48°N shows two features: (i) a sudden shift in probability of a decline in transport (reaching a 95% probability of a 20-

year declining trend, with a 56% probability of an intense AMOC decrease), and (ii) the strongest forced trend (-0.11 Sv psu yr^{-1}) relative to the full 250-year timeseries. To explore the cause and consequences of this unique event, this section investigates whether there is also a change in behaviour in the forced component of salinity transports over this period, for direct timing comparison to the AMOC (Figures 12 and 13). Note that a 20-year trend (here denoted as $\Theta\mathscr{S}$) in 1995, for example, refers to a linear regression from 1985 to 2005 in this study.

The 20-year trends of the ensemble mean salinity transport in the SPR ($\Theta\mathscr{S}|_{\mathrm{SP}}$) are consistently negative over the unique event (Figure 12b). This feature is not seen over any other 20-year period throughout the 250-year timeseries of historical and RCP8.5 data output. This is consistent with findings in Holliday et al (2020) that from 2012 to 2016, a unique extreme freshening occurred in the eastern SPR that had not previously been seen in 120 years of observations. In our results, almost simultaneously, both ΘAMOC and $\Theta\mathscr{S}|_{\mathrm{SP}}$ 20-year declines fall outside the variability found during their historical period. Furthermore, the 20-year trend around 2001 (from 1991 to 2011) marks the maximum net salinity decline in the trend (of -0.051 Sv psu yr^{-1}). Changes in STR transport trends do not seem exclusive to the unique event and therefore the SPR remains the point of focus.

For a deeper analysis, to investigate whether this subpolar salinity unique event is mostly linked to ocean or atmospheric fluxes, $\Theta_{\mathrm{ov}}|_{\mathrm{SP}}$, $\Theta_{\mathrm{az}}|_{\mathrm{SP}}$, and $\Theta\mathscr{F}|_{\mathrm{SP}}$ are used. It becomes evident that the subpolar oceanic transport components of salinity demonstrate a behaviour that is unique to this period. In the first seven years (1995 to 2002), $\Theta_{\mathrm{az}}|_{\mathrm{SP}}$ 20-year trends are negative, and soon after in 1998, $\Theta_{\mathrm{ov}}|_{\mathrm{SP}}$ trends change to a negative sign (reaching the 250-year minimum in 2008, of -0.064 Sv psu yr^{-1}), and then sustaining a decline until the end of the unique event (Figure 12b). This is caused by an average divergence of salinity by $\Theta_{\mathrm{ov}}|_{\mathrm{SP}}$, with both $\Theta_{\mathrm{ov}}|_{48N}$ and $\Theta_{\mathrm{ov}}|_{60N}$ exporting salt out of the SPR (Figure 13). The maximum net salinity transport decline in 2001 (as mentioned above) coincides with an overlap of a 20-year negative trend shared by $\Theta_{\mathrm{ov}}|_{\mathrm{SP}}$ and $\Theta_{\mathrm{az}}|_{\mathrm{SP}}$ of -0.025 Sv psu yr^{-1}. This is unprecedented and not repeated after the unique event since Θ_{ov} and Θ_{az} normally complement each other, in that one transport component increases while the other decreases (both in the historical and future scenario).

The 20-year atmospheric salinity transport trends $\Theta\mathscr{F}|_{\mathrm{SP}}$, on the other hand, do not show any anomalous feature during the unique event, with positive and negative trend oscillations occurring consistently over the 250 years (Figure 12b). Its average trend over the unique event is negligible (Figure 13). These results illustrate that on this short (interdecadal) period, the oceanic internal processes, such as the overturning and gyre circulation, largely dominate over the effects of atmospheric fluxes to set the forced component of the salinity changes consistent with an AMOC reduction.

5 Conclusion

Following the IPCC's findings that the AMOC is very likely to experience a decline in transport in the 21$^{\mathrm{st}}$ century (Flato et al, 2013), this study quantifies the decline in past and future strength of the AMOC at 48°N over 250 years. Trends of different lengths, covering interannual to multi-decadal timescales, are analysed to reveal that under both future scenarios used (RCP4.5 and RCP8.5), the forcing is only detected outside the range of intrinsic variability for a consistent decline longer than 5 years. This suggests that any interannual intense events, such as the 2009-2010 30% decline in transport recorded by RAPID (Bryden et al, 2014), are more akin to intrinsic variability rather than forced long-term decline. The results also imply that there was a high probability (up to 85% at the turn of the century, in RCP8.5) of seeing a weak decadal decline, such as that seen in RAPID (Smeed et al, 2014), due to forcing. A decadal trend could still be dominated by intrinsic variability as suggested by Roberts et al (2014), which is characterised as a hiatus in Sévellec et al (2016). Upon increasing the time-duration of the forced trends, stronger intensities and probabilities of a decline are seen (86% time-average probability of an intense 40-year decline under RCP8.5). Using time-varying forced trends, the 'business-as-usual' scenario shows a sustained high probability of a decline in the AMOC, whereas the 'stabilisation' scenario returns to pre-industrial probabilities of an equal chance in increasing or decreasing (for all trend durations over 5 years).

From 1995 to 2015, a unique event is identified by features of the timeseries that are unique to this timeframe: (i) a rapid increase in probability of a decline in AMOC transport (from the historical average probability of 50% to 95% for a 20-year RCP8.5 negative trend), and (ii) the strongest forced-trend intensity of the full 250-year timeseries is detected (-0.11 Sv yr^{-1}). Based on these initial results showing the fundamental role of forced-variation, we investigated whether forced changes in the AMOC trends coincide with forced changes in oceanic properties, namely temperature and salinity transport. The focus here is on the positive feedback of salinity transport; a decline in the AMOC decreases salt transport to higher latitudes, which reduces NADW formation and further slows down the AMOC (Marotzke, 1996). The stability of the AMOC is dependent on a complex salinity balance resulting from freshwater or salinity transport by the gyre circulation, the meridional overturning circulation, and atmospheric fluxes (Rahmstorf, 1996), hence the reason for estimating these three transports from ensemble mean salinity budgets in the subpolar and subtropical regions. After establishing the average salinity transports during a period close to AMOC equilibrium (from 1850 to 1975), two anomalous cases are analysed: (i) the long-term accumulated anomalies of salinity transports after 125 years (1975 to 2099), and (ii) the 20-year salinity transport trends over the unique event identified (1995 to 2015).

In the first case, a meridional dipole in salinity forms after 1975 and intensifies until the end of the 21$^{\text{st}}$ century. It is characterised by a fresher SPR and saltier STR. This results in an accumulated decrease in salinity of $+0.03$ psu and increase of $+0.09$ psu by 2095 in the SPR and STR, respectively. It is only when expressing these salinity changes as ensemble means that the signal is detected; even though the change is on the order of <0.1 psu, the salinity budget is affected. The sustained increase in salt in the STR is influenced by both oceanic components, where the overturning circulation ($\Delta\mathscr{S}_{\text{ov}}|_{ST}$) dominates the import of salt from 1975 to 2050 and then horizontal circulation ($\Delta\mathscr{S}_{\text{az}}|_{ST}$), over the last 50 years. The SPR's accumulated negative transport of salt from 2020 to 2099 is a result of the shared impact of both overturning and horizontal circulations ($\Delta\mathscr{S}_{\text{ov}}|_{SP}$ and $\Delta\mathscr{S}_{\text{az}}|_{SP}$, respectively), exporting salt out of the SPR. When comparing the long-term effects of the ocean circulation ($\Delta\mathscr{S}_{\text{ov}}+\Delta\mathscr{S}_{\text{az}}|_{ST}$) compared to the ones of the atmospheric flux ($\mathscr{F}|_{ST}$), their accumulated transports are almost identical through time, hence the accumulation of salt is caused by both evaporation and ocean export. The SPR completely relies on the oceanic components to produce net negative salinity transport by 2099, since the atmospheric forcing causes positive transport (net decrease in precipitation) in the model ensemble. The divergence of salt transport by the ocean circulation ($\Delta\mathscr{S}_{\text{ov}}+\Delta\mathscr{S}_{\text{az}}$) and hence the AMOC slowdown through the positive feedback in the subpolar region is therefore the dominant driver on multi-decadal to centennial timescales, overriding atmospheric effects; this is consistent with results from other studies (Manabe and Stouffer, 1988; Rahmstorf, 1996).

The 20-year unique event of the AMOC decline from 1995 to 2015 coincides with changes in the 20-year subpolar trends of salinity transport that occur exclusively during this period. Yeager and Danabasoglu (2014) demonstrate that the AMOC's decadal variability mainly responds to high-latitude buoyancy forcing anomalies, and results here demonstrate a similar response over decadal abrupt periods. Robson et al (2016) identified negative (light) density anomalies in the deep Labrador Sea related to ocean warming and coinciding with an AMOC decline from 1995 to 2015. However, compared to waters in the 1970s, waters in 2015 were not warmer but rather fresher. This suggests that although the salinity changes are smaller than temperature changes, the accumulated effects of freshwater increase played a significant role on buoyancy and therefore AMOC transport from the 1970s to 2010s (Robson et al, 2016).

The results here extend further in time, showing that the 1995-2015 period is the only 20-year period over 250 years (1850-2100) that has a continuously-negative forced-trend in total SPR salinity transport. Holliday et al (2020) also define a period between 2012 and 2016 when an extreme freshening occurred in the eastern SPR relative to 120 years of observations. We show that this unique event coincides with a period of high probability of strong AMOC decline driven by the forced component. In this context, our study additionally separates forced and intrinsic variations. Here, we show the components that drive the changes are initiated by a decline in the salinity transport associated with the horizontal circulation ($\Theta_{\text{az}}|_{SP}$) and sustained by a subsequent decline in the

overturning circulation ($\Theta_{\mathrm{ov}}|_{SP}$). It is worth noting that it is during this unique event (1995-2015) that the salt export by the overturning circulation reaches its maximum declining trend ($\Theta_{\mathrm{ov}}|_{SP}$) relative to the full timeseries in 2008.

One specific year during the unique event, 2001 (i.e., 20 year trends from 1991 to 2011), marks two unique features that happen simultaneously: (i) The strongest net trend in salinity transport in the SPR ($\Theta\mathscr{S}|_{SP}$) in 250 years is achieved (-0.051 Sv psu yr^{-1}), (ii) negative 20-year trends due to both overturning and horizontal circulation in the SPR ($\Theta_{\mathrm{ov}}|_{SP}$ and $\Theta_{\mathrm{az}}|_{SP}$, respectively) overlap at -0.02 Sv psu yr^{-1}, and (iii) the difference between the SPR declining trend in salinity transport ($\Theta\mathscr{S}|_{SP}$) and STR ($\Theta\mathscr{S}|_{ST}$) increasing trend is largest. The latter point has been extensively studied previously, wherein alterations to the large-scale meridional density gradient between the North Atlantic gyres affects the AMOC (Zhang, 2010; Robson et al, 2014; McCarthy et al, 2015; Yeager and Danabasoglu, 2014; Sévellec and Huck, 2016). The collective effect of these features happening in parallel could be the explanation for a shift in probability of an AMOC decline due to forced variations. On this decadal timescale, the atmospheric flux term (computed as the residual term in our study) has a negligible effect on the salinity of the unique event since there is no anomalous increase in evaporation in the STR, nor precipitation in the SPR and therefore the results suggest that the joint overturning and horizontal circulation term ($\mathscr{S}_{\mathrm{ov}} + \mathscr{S}_{\mathrm{az}}$) dominates the forced salinity transport over 20-year timescales.

It is commonly accepted that numerical model outputs exhibit a degree of inherent uncertainty, which is addressed in this study by using the ensemble mean (both for the forced component and the PDF of the intrinsic variability) to mitigate errors and bias found in single models. Nevertheless, it is challenging to compare these results to observations due to sparsity of direct salinity or freshwater transport estimates (Talley, 2008; Liu et al, 2014; McDonagh et al, 2010). Several studies have therefore used numerical models, following the similar computations as this study, to generate freshwater flux estimates (referred to as Mov and Maz, for the overturning and horizontal component, respectively, e.g., de Vries and Weber, 2005; Bryden et al, 2011; Drijfhout et al, 2011; McDonagh et al, 2015; Mecking et al, 2016, 2017). Although the budget shows that net evaporation over the Atlantic basin is required (Drijfhout et al, 2011), a thorough analysis to understand CMIP5 biases in Mecking et al (2017) demonstrate that evaporation could be overestimated over the North Atlantic in the models, compared to available observations, reanalysis products, and other models. This could both affect our results and potentially change the lack of intensification of the water cycle under anthropogenic climate change. An increase in CO_2 concentrations should increase absolute atmospheric humidity and increase poleward water vapour transport, therefore increasing precipitation (Manabe and Stouffer, 1994, 1999). Furthermore, as mentioned in the Methods, we regrid the original CMIP5 model data to a nearest even-numbered coordinate, which could result in uncertainties related to mass conservation and hence the residual calculations. A follow-up study could be performed to test the sensitivity of our results to estimated biases or re-gridding choices.

Finally, this study highlights the potential use of a similar decomposition into horizontal and overturning transports of salinity for improving the skill of interdecadal predictions. For example, if these unique event features are a robust identification of a shift towards a sustained probability of an AMOC decline, then identifying shifts in salinity transports leading to more sustained changes in the AMOC may be possible. A complete collapse of the AMOC is highly unlikely to occur in the 21$^{\mathrm{st}}$ century, due to the order of magnitude of changes in salinity in CMIP5 being too small (Stocker et al, 2013). Nevertheless, a rapid shift to a long decadal transient decline in the AMOC can also have drastic effects on the localised and global climate system (Vellinga and Wood, 2002). There is therefore a need for a constant improved understanding of early warning signs of an AMOC decline (Boulton et al, 2014). Despite being focused on the forced component, this study proposes that with further analysis, such a proxy could be achieved from identifying concurrent changes in the 20-year AMOC and salinity transport trends. Such an understanding can be used to improve future climate risk mitigation strategies and planning, with global socio-economic importance in the 21st century.

Acknowledgements We would like to thank and acknowledge the World Climate Research Programme's Working Group on Coupled Modelling, which is responsible for CMIP. We would also like to thank Jenny Mecking and Clément Vic for their help with the pre-processing of CMIP5 data and salinity budget computations, respectively.

References

Bakker P, Schmittner A, Lenaerts JTM, Abe-Ouchi A, Bi D, van den Broeke MR, Chan WL, Hu A, Beadling RL, Marsland SJ, Mernild SH, Saenko OA, Swingedouw D, Sullivan A, Yin J (2016) Fate of the Atlantic Meridional Overturning Circulation: Strong decline under continued warming and Greenland melting. Geophysical Research Letters 43(23):12252–12260, DOI 10.1002/2016GL070457

Baumgartner A, Reichel E (1975) The World Water Balance: Mean Annual Global, Continental and Maritime Precipitation, Evaporation and Run-off. Elsevier Scientific, New York p 179

Bond GC, Showers W, Elliot M, Evans M, Lotti R, Hajdas I, Bonani G, Johnson S (1999) The North Atlantic's 1-2 kyr Climate Rhythm: Relation to Heinrich Events, Dansgaard/Oeschger Cycles and the Little Ice Age. Geophysical Monograph Series 112:35–58, DOI 10.1029/GM112p0035

Böning CW, Behrens E, Biastoch A, Getzlaff K, Bamber JL (2016) Emerging impact of Greenland meltwater on deepwater formation in the North Atlantic Ocean. Nature Geoscience 9(7):523–527, DOI 10.1038/ngeo2740

Boulton CA, Allison LC, Lenton TM (2014) Early warning signals of Atlantic Meridional Overturning Circulation collapse in a fully coupled climate model. Nature Communications 5(7):5752, DOI 10.1038/ncomms6752

Broecker WS (1998) Paleocean circulation during the Last Deglaciation: A bipolar seesaw? Paleoceanography 13(2):119–121, DOI 10.1029/97PA03707

Broecker WS, Peteet DM, Rind D (1985) Does the ocean-atmosphere system have more than one stable mode of operation? Nature 315(2):21–26, DOI 10.1038/315021a0

Bryden HL, King BA, Mccarthy GD (2011) South Atlantic overturning circulation at 24S. Journal of Marine Research 69(1):39–56, DOI 10.1357/002224011798147633

Bryden HL, King BA, McCarthy GD, McDonagh EL (2014) Impact of a 30in Atlantic meridional overturning during 2009-2010. Ocean Science 10(4):683–691, DOI 10.5194/os-10-683-2014

Buckley MW, Marshall J (2016) Observations, inferences, and mechanisms of the Atlantic Meridional Overturning Circulation: A review. Reviews of Geophysics 54:5–63, DOI 10.1002/2015RG000493

Caesar L, McCarthy G, Thornalley D, Cahill N, Rahmstorf S (2021) Current atlantic meridional overturning circulation weakest in last millennium. Nature Geoscience 14(3):118–120, DOI 10.1038/s41561-021-00699-z

Dansgaard W, Johnsen SJ, Clausen HB, Dahl-Jensen D, Gundestrup NS, Hammer CU, Hvidberg CS, Steffensen JP, Sveinbjörnsdottir AE, Jouzel J, Bond G (1993) Evidence for general instability of past climate from a 250-kyr ice-core record. Nature 364:218–220, DOI 10.1038/364218a0

Delworth TL, Zhang R, Mann ME (2007) Decadal to Centennial Variability of the Atlantic From Observations and Models. Ocean Circulation: Mechanisms and Impacts 173:131–148, DOI 10.1029/173GM10

Dickson B, Yashayaev I, Meincke J, Turrell B, Dye S, Holfort J (2002) Rapid freshening of the deep North Atlantic Ocean over the past four decades. Nature 416(6883):832–837, DOI 10.1038/416832a

Dijkstra HA (2007) Characterization of the multiple equilibria regime in a global ocean model. Tellus A: Dynamic Meteorology and Oceanography 59(5), DOI 10.1111/j.1600-0870.2007.00267.x

Drijfhout S, Jan van Oldenborgh G, Cimatoribus A (2012) Is a Decline of AMOC Causing the Warming Hole above the North Atlantic in Observed and Modeled Warming Patterns? Journal of Climate 25:8373–8379, DOI 10.1175/JCLI-D-12-00490.1

Drijfhout SS, Weber SL, Swaluw EVD (2011) The stability of the MOC as diagnosed from model projections for pre-industrial, present and future climates. Climate Dynamics 37(7-8):1575–1586, DOI 10.1007/s00382-010-0930-z

Easterling DR, Wehner MF (2009) Is the climate warming or cooling? Geophysical Research Letters 36(8):4–6, DOI 10.1029/2009GL037810

Ezer T (2015) Detecting changes in the transport of the Gulf Stream and the Atlantic overturning circulation from coastal sea level data: The extreme decline in 2009-2010 and estimated variations for 1935-2012. Global and Planetary Change 129:23–36, DOI 10.1016/j.gloplacha.2015.03.002

Flato G, Marotzke J, Abiodun B, Braconnot P, Chou S, Collins W, Cox P, Driouech F, Emori S, Eyring V, Forest C, Gleckler P, Guilyardi E, Jakob C, Kattsov V, Reason C, Rummukainen M (2013) IPCC 2013 AR5 - Chapter 9: Evaluation of Climate Models. In: Climate Change 2013: The Physical Science Basis. Contribution of Working Group I to the Fifth Assessment Report of the Intergovernmental Panel on Climate Change, pp 741–866, DOI 10.1017/CBO9781107415324, arXiv:1011.1669v3

Ganachaud A, Wunsch C (2003) Large-Scale Ocean Heat and Freshwater Transports during the World Ocean Circulation Experiment. Journal of Climate 16:696–705, DOI 10.1175/1520-0442(2003)016⟨0696:LSOHAF⟩2.0.CO;2

Gregory JM, Dixon KW, Stouffer RJ, Weaver AJ, Driesschaert E, Eby M, Fichefet T, Hasumi H, Hu A, Jungclaus JH, Kamenkovich IV, Levermann A, Montoya M, Murakami S, Nawrath S, Oka A, Sokolov AP, Thorpe RB (2005) A model intercomparison of changes in the Atlantic thermohaline circulation in response to increasing atmospheric CO_2 concentration. Geophysical Research Letters 32:1–5, DOI 10.1029/2005GL023209

Hall MM, Bryden HL (1982) Direct estimates and mechanisms of ocean heat transport. Deep Sea Research Part A, Oceanographic Research Papers 29(3):339–359, DOI 10.1016/0198-0149(82)90099-1

Holliday NP, Bersch M, Berx B, Chafik L, Cunningham S, Florindo-López C, Hátún H, Johns W, Josey SA, Larsen KMH, et al (2020) Ocean circulation causes the largest freshening event for 120 years in eastern subpolar north atlantic. Nature communications 11(1):1–15, DOI 10.1038/s41467-020-14474-y

Hu A, Meehl Ga, Han W, Yin J (2009) Transient response of the MOC and climate to potential melting of the Greenland Ice Sheet in the 21st century. Geophysical Research Letters 36(April):1–6, DOI 10.1029/2009GL037998

Huang B, Hu ZZ, Schneider EK, Wu Z, Xue Y, Klinger B (2012a) Influences of tropical-extratropical interaction on the multidecadal AMOC variability in the NCEP climate forecast system. Climate Dynamics 39(3-4):531–555, DOI 10.1007/s00382-011-1258-z

Huang B, Xue Y, Kumar A, Behringer DW (2012b) AMOC variations in 1979 – 2008 simulated by NCEP operational ocean data assimilation system. Climate Dynamics 38(3):513–525, DOI 10.1007/s00382-011-1035-z

Jackson LC, Peterson KA, Roberts CD, Wood RA (2016) Recent slowing of Atlantic overturning circulation as a recovery from earlier strengthening. Nature Geoscience 9(7):518–522, DOI 10.1038/ngeo2715

Josey SA, Marsh R (2005) Surface freshwater flux variability and recent freshening of the North Atlantic in the eastern subpolar gyre. Journal of Geophysical Research 110:1–17, DOI 10.1029/2004JC002521

Latif M, Roeckner E, Mikolajewicz U, Voss R (2000) Tropical Stabilization of the Thermohaline Circulation in a Greenhouse Warming Simulation. Journal of Climate 13(11):1809–1813, DOI 10.1175/1520-0442(2000)013⟨1809%3AL⟩2.0.CO%3B2

Liu W, Liu Z, Brady EC (2014) Why is the AMOC Monostable in Coupled General Circulation Models? Journal of Climate 27(6):2427–2443, DOI 10.1175/JCLI-D-13-00264.1

Manabe S, Stouffer RJ (1988) Two Stable Equilibria of a Coupled Ocean-Atmosphere Model. Journal of Climate 1:841–866, DOI 10.1175/1520-0442(1988)001⟨0841:TSEOAC⟩2.0.CO;2

Manabe S, Stouffer RJ (1994) Multiple-century response of a coupled ocean-atmosphere model to an increase of atmospheric carbon dioxide. Journal of climate 7(1):5–23, DOI 10.1175/1520-0442(1994)007⟨0005:MCROAC⟩2.0.CO;2

Manabe S, Stouffer RJ (1999) The role of thermohaline circulation in climate. Tellus B : Chemical and Physical Meteorology 51(1):91–109, DOI 10.3402/tellusb.v51i1.16262

Marotzke J (1996) Analysis of thermohaline feedbacks. In: Decadal Climate Variability, Springer, Berlin, Heidelberg, pp 333–378

McCarthy G, Frajka-Williams E, Johns WE, Baringer MO, Meinen CS, Bryden HL, Rayner D, Duchez A, Roberts C, Cunningham SA (2012) Observed interannual variability of the Atlantic meridional overturning circulation at 26.5°N. Geophysical Research Letters 39(19):1–5, DOI 10.1029/2012gl052933

McCarthy GD, Haigh ID, Hirschi JJM, Grist JP, Smeed DA (2015) Ocean impact on decadal Atlantic climate variability revealed by sea-level observations. Nature 521:508–523, DOI 10.1038/nature14491

McDonagh EL, McLeod P, King BA, Bryden HL, Torres Valdes S (2010) Circulation, Heat, and Freshwater Transport at 36N in the Atlantic. Journal of Physical Oceanography 40:2661–2678, DOI 10.1175/2010JPO4176.1

McDonagh EL, King BA, Bryden HL, Courtois P, Szuts Z, Baringer M, Cunningham SA, Atkinson C, McCarthy G (2015) Continuous Estimate of Atlantic Oceanic Freshwater Flux at 26.5N. Journal of Climate 28(22):8888–8906, DOI 10.1175/JCLI-D-14-00519.1

Mecking J, Drijfhout SS, Jackson LC, The MBA (2017) The effect of model bias on Atlantic freshwater transport and implications for AMOC bi-stability. Tellus A: Dynamic Meteorology and Oceanography 69:1–15, DOI 10.1080/16000870.2017.1299910

Mecking JV, Drijfhout SS, Jackson LC, Graham T (2016) Stable AMOC off state in an eddy-permitting coupled climate model. Climate Dynamics 47(7-8):2455–2470, DOI 10.1007/s00382-016-2975-0

Moat BI, Smeed DA, Frajka-Williams E, Desbruyères DG, Beaulieu C, Johns WE, Rayner D, Sanchez-Franks A, Baringer MO, Volkov D, et al (2020) Pending recovery in the strength of the meridional overturning circulation at 26n. Ocean Science 16(4):863–874, DOI 10.5194/os-16-863-2020

Parker A, Ollier CD (2016) There is no real evidence for a diminishing trend of the Atlantic meridional overturning circulation. Journal of Ocean Engineering and Science 1(1):30–35, DOI 10.1016/j.joes.2015.12.007

Pohlmann H, Sienz F, Latif M (2006) Influence of the Multidecadal Atlantic Meridional Overturning Circulation Variability on European Climate. Journal of Climate-Special Section 19:6062–6067, DOI 10.1175/JCLI3941.1

Rahmstorf S (1995) Bifurcations of the Atlantic thermohaline circulation in response to changes in the hydrological cycle. Nature 378(6553):145–149, DOI 10.1038/378145a0

Rahmstorf S (1996) On the freshwater forcing and transport of the Atlantic thermohaline circulation. Climate Dynamics 12(12):799–811, DOI 10.1007/s003820050144

Rahmstorf S (2000) The thermohaline ocean circulation: A system with dangerous thresholds? Climatic Change 46(3):247–256, DOI 10.1023/A:1005648404783

Rahmstorf S, Box JE, Feulner G, Mann ME, Robinson A, Rutherford S, Schaffernicht EJ (2015) Exceptional twentieth-century slowdown in Atlantic Ocean overturning circulation. Nature Climate Change 5(5):475–480, DOI 10.1038/nclimate2554

Roberts CD, Jackson L, McNeall D (2014) Is the 2004-2012 reduction of the Atlantic meridional overturning circulation significant? Geophysical Research Letters 41(9):3204–3210, DOI 10.1002/2014GL059473.1.

Robson J, Hodson D, Hawkins E, Sutton R (2014) Atlantic Overturning in decline? Nature 7(1):2–3, DOI 10.1038/ngeo2050

Robson J, Ortega P, Sutton R (2016) A reversal of climatic trends in the North Atlantic since 2005. Nature Geoscience 9(7):513–517, DOI 10.1038/ngeo2727

Schleussner CF, Levermann A, Meinschausen M (2014) Probabilistic projections of the Atlantic overturning. Climatic Change 127(3-4):579–586, DOI 10.1007/s10584-014-1265-2

Schmittner A, Latif M, Schneider B (2005) Model projections of the North Atlantic thermohaline circulation for the 21st century assessed by observations. Geophysical Research Letters 32(23):1–4, DOI 10.1029/2005GL024368

Sévellec F, Fedorov AV (2011) Stability of the Atlantic meridional overturning circulation and stratification in a zonally averaged ocean model: Effects of freshwater flux, Southern Ocean winds, and diapycnal diffusion. Deep-Sea Research Part II: Topical Studies in Oceanography 58(17-18):1927–1943, DOI 10.1016/j.dsr2.2010.10.070

Sévellec F, Huck T (2016) Geostrophic Closure of the Zonally Averaged Atlantic Meridional Overturning Circulation. Journal of Physical Oceanography 46(3):895–917, DOI 10.1175/JPO-D-14-0148.1

Sévellec F, Sinha B, Skliris N (2016) The rogue nature of hiatuses in a global warming climate. Geophysical Research Letters 43(15):8169–8177, DOI 10.1002/2016GL068950

Sévellec F, Federov AV, Liu W (2017) Arctic sea ice decline weakens the Atlantic Meridional Overturning Circulation. Nature Climate Change 7:604–610, DOI 10.1038/nclimate3353

Smeed D, McCarthy G, Cunningham S, Frajka-Williams E, Rayner D, Johns W, Meinen C, Baringer M, Moat B, Duchez A, Bryden H (2013) Observed decline of the Atlantic Meridional Overturning Circulation 2004 to 2012. Ocean Science Discussions 10(5):1619–1645, DOI 10.5194/osd-10-1619-2013

Smeed DA, McCarthy GD, Cunningham SA, Frajka-Williams E, Rayner D, Johns WE, Meinen CS, Baringer MO, Moat BI, Duchez A, Bryden HL (2014) Observed decline of the Atlantic meridional overturning circulation 2004 - 2012. Ocean Science 10:29–38, DOI 10.5194/os-10-29-2014

Smeed DA, Josey SA, Beaulieu C, Johns WE, Moat BI, Frajka-Williams E, Rayner D, Meinen CS, Baringer MO, Bryden HL, McCarthy GD (2018) The North Atlantic Ocean is in a state of reduced overturning. Geophysical Research Letters 45(3):1527–1533, DOI 10.1002/2017GL076350

Srokosz M, Baringer M, Bryden H, Cunningham S, Delworth T, Lozier S, Marotzke J, Sutton R (2012) Past, Present, and Future Changes in the Atlantic Meridional Overturning Circulation. Bulletin of the American Meteorological Society 93(11):1663–1676, DOI 10.1175/bams-d-11-00151.1

Stocker T, Qin D, Plattner G, Tignor M, Allen S, Boschung J, Nauels A, Xia Y, Bex V, Midgley P (2013) Summary for Policymakers. In: Climate Change 2013: The Physical Science Basis.Contribution of Working Group I to the Fifth Assessment Report of the Intergovernmental Panel on Climate Change, Cambridge University Press, Cambridge, UK, and New York, USA, pp 3–29, DOI 10.1017/CBO9781107415324.004

Stommel H (1961) Thermohaline convection with two stable regimes. Tellus 13(2):224–230, DOI 10.1111/j.2153-3490.1961.tb00079.x

Stouffer R, Yin J, Gregory J, Dixon K, Spelman M, Hurlin W, Weaver A, Eby M, Flato G, Hasumi H, Hu A, Jungclaus J, Kamenkovich IV, Levermann A, Montoya M, Mukarami S, Nawrath S, Oka A, Peltier WR, Robitaille DY, Sokolov A, Vettoretti G, Weber SL (2006) Investigating the Causes of the Response of the Thermohaline Circulation to Past and Future Climate Change. Journal of Climate 19(8):1365–1387, DOI 10.1175/JCLI3689.1

Talley LD (2008) Freshwater transport estimates and the global overturning circulation: Shallow, deep and throughflow components. Progress in Oceanography 78:257–303, DOI 10.1016/j.pocean.2008.05.001

Thorpe RB, Gregory JM, Johns TC, Wood RA, Mitchell JFB (2001) Mechanisms Determining the Atlantic Thermohaline Circulation Response to Greenhouse Gas Forcing in a Non-Flux-Adjusted Coupled Climate Model. Journal of Climate 14(14):3102–3116, DOI 10.1175/1520-0442(2001)014⟨3102:MDTATC⟩2.0.CO;2

Urban NM, Keller K (2010) Probabilistic hindcasts and projections of the coupled climate, carbon cycle and Atlantic meridional overturning circulation system: A Bayesian fusion of century-scale observations with a simple model. Tellus, Series A: Dynamic Meteorology and Oceanography 62(5):737–750, DOI 10.1111/j.1600-0870.2010.00471.x

Vellinga M, Wood RA (2002) Global Climatic Impacts of a Collapse of the Atlantic Thermohaline Circulation. Climatic Change 54:251–267, DOI 10.1023/A:1016168827653

de Vries P, Weber SL (2005) The Atlantic freshwater budget as a diagnostic for the existence of a stable shut down of the meridional overturning circulation. Geophysical Research Letters 32(9):1–4, DOI 10.1029/2004GL021450

Weaver AJ, Sedláček J, Eby M, Alexander K, Crespin E, Fichefet T, Philippon-Berthier G, Joos F, Kawamiy M, Matsumoto K, Steinacher M, Tachiiri K, Tokos K, Yoshimori M, Zickfeld K (2012) Stability of the Atlantic meridional overturning circulation: A model intercomparison. Geophysical Research Letters 39(20):1–8, DOI 10.1029/2012GL053763

Wood RA, Keen AB, Mitchell JFB, Gregory JM, Wood RA, Keen AB, Mitchell JFB, Gregory JM (1999) Changing spatial structure of the thermohaline circulation in response to atmospheric CO_2 forcing in a climate model. Nature 399:572–575, DOI 10.1038/21170

Worthington EL, Moat BI, Smeed DA, Mecking JV, Marsh R, McCarthy GD (2021) A 30-year reconstruction of the atlantic meridional overturning circulation shows no decline. Ocean Science 17(1):285–299, DOI 10.5194/os-17-285-2021

Yeager S, Danabasoglu G (2014) The origins of late-twentieth-century variations in the large-scale North Atlantic circulation. Journal of Climate 27:3222–3247, DOI 10.1175/JCLI-D-13-00125.1

Zhang R (2010) Latitudinal dependence of Atlantic meridional overturning circulation (AMOC) variations. Geophysical Research Letters 37:1–6, DOI 10.1029/2010GL044474

Zhang R, Delworth T (2005) Simulated Tropical Response to a Substantial Weakening of the Atlantic Thermohaline Circulation. Journal of Climate 18:1853–1860, DOI 10.1175/JCLI3460.1

Statements and Declarations

Funding

This study was jointly funded by the department of Ocean and Earth Science, University of Southampton and the National Physical Laboratory. The research at the National Physical Laboratory was funded by the National Metrology Programme of the UK Department of Business, Energy and Industrial Strategy (BEIS). This research was also supported by the UK Natural and Environmental Research Council (SMURPHS, NE/N005767/1) and by the DECLIC project funded through the French CNRS/INSU/LEFE program.

Competing interests

The authors declare that there are no competing interests.

Author Contributions

All authors contributed to the study conception and design. Material preparation, and analysis were performed by Delphine Lobelle, with frequent feedback from Florian Sévellec. The first draft of the manuscript was written by Delphine Lobelle and all authors read, edited and approved the final manuscript.

Data availability

The Coupled Model Intercomparison Project Phase 5 (CMIP5) data can be found from the portal Earth System Grid - Center for Enabling Technologies (ESG-CET), on https://esgf-node.llnl.gov/search/cmip5/.

List of Figures

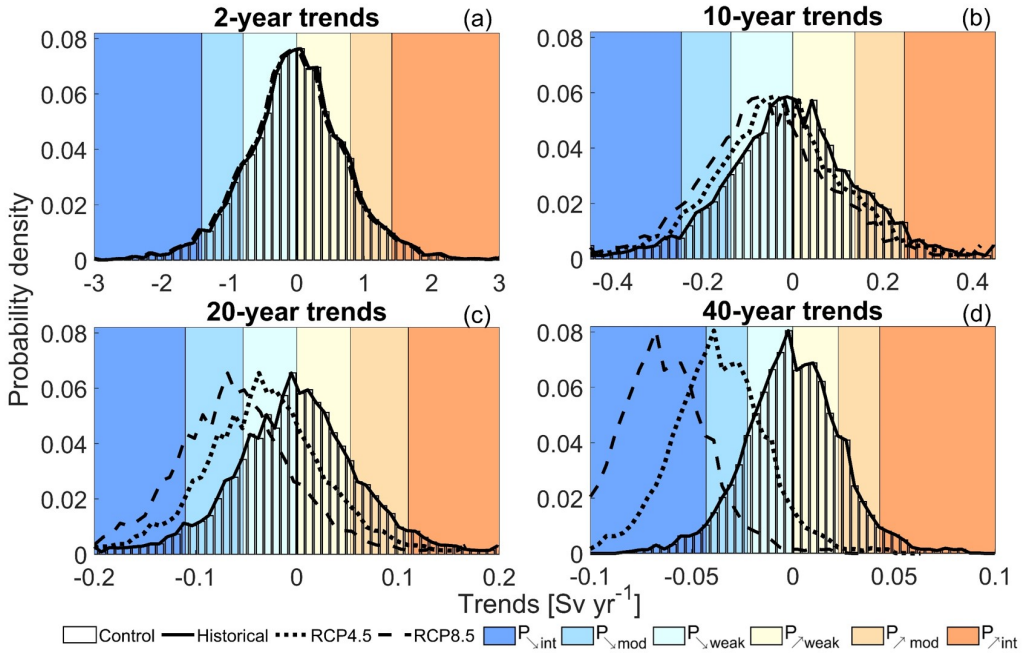

Fig. 1 Probability density functions of the 48°N AMOC's intrinsic variability, from the control simulations (vertical bar-plots), intrinsic variability plus historical time-mean forced variability (solid lines), intrinsic variability plus RCP4.5 time-mean forced varaibility (dotted lines), intrinsic variability plus RCP8.5 time-mean forced variability (dashed lines) using different time-mean trend durations: (a) 2 years, (b) 10 years, (c) 20 years, and (d) 40 years. The colours represent the six categories of trend probabilities: intense decrease (P_{int-}) and intense increase (P_{int+}), for the area >2 standard deviations in dark blue and dark orange, respectively, moderate decrease (P_{mod-}) and moderate increase (P_{mod+}), for the area between 1 and 2 standard deviations in light blue and light orange, respectively, and weak decrease (P_{weak-}) and weak increase (P_{weak+}), for the area between 0 and 1 standard deviations in pale blue and yellow, respectively

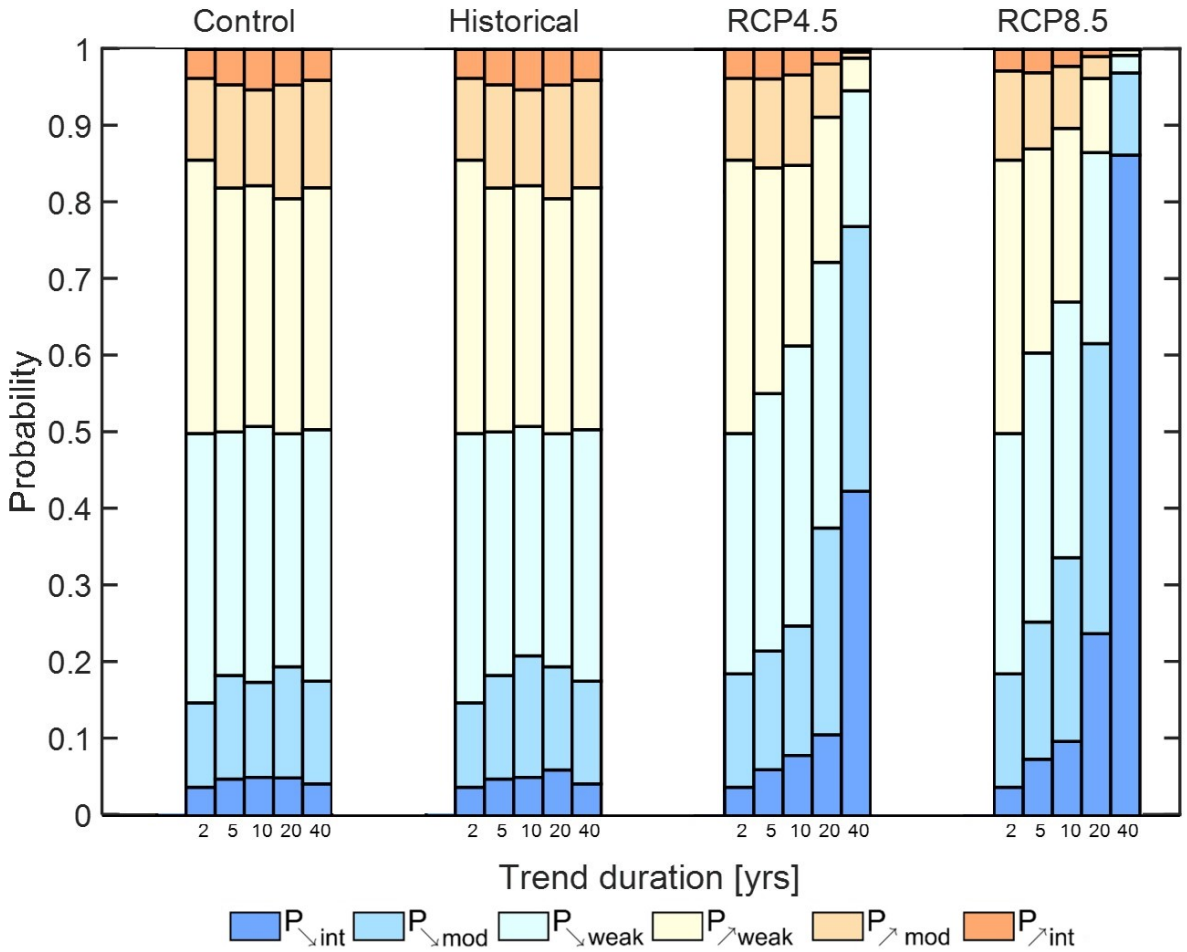

Fig. 2 Probabilities of trends of the intrinsic variability or intrinsic variability plus time-mean forced variability for the six probability categories defined in Equation 1. Here, some additional trend durations are also included (1, 2, 5, 10, 20 and 40 years). The different scenarios are grouped together and labelled above: control (pre-industrial simulations), historical (from 1850 to 2005), and RCP4.5 and RCP8.5 (both from 2006 to 2099)

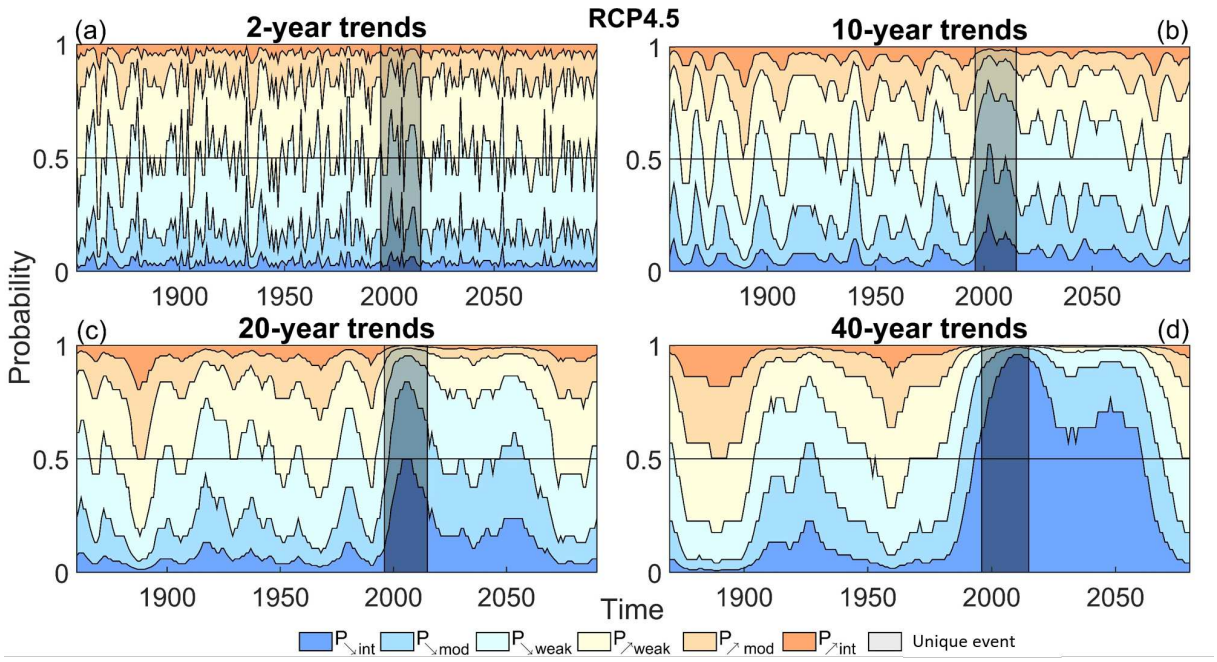

Fig. 3 Probability of events over the historical and future RCP4.5 periods. The time-varying ensemble mean probabilities of the intrinsic variability plus forced variability over the historical and future scenario of the AMOC at 48°N, from 1850 to 2099. The trends are filtered over different trend durations: (a) 2 years, (b) 10 years, (c) 20 years, and (d) 40 years. The unique event from 1995 to 2015 representing the maximum 20-year AMOC decline probability is shaded in grey. The six colours display the six probability categories defined in Equation 1 and Figure 1

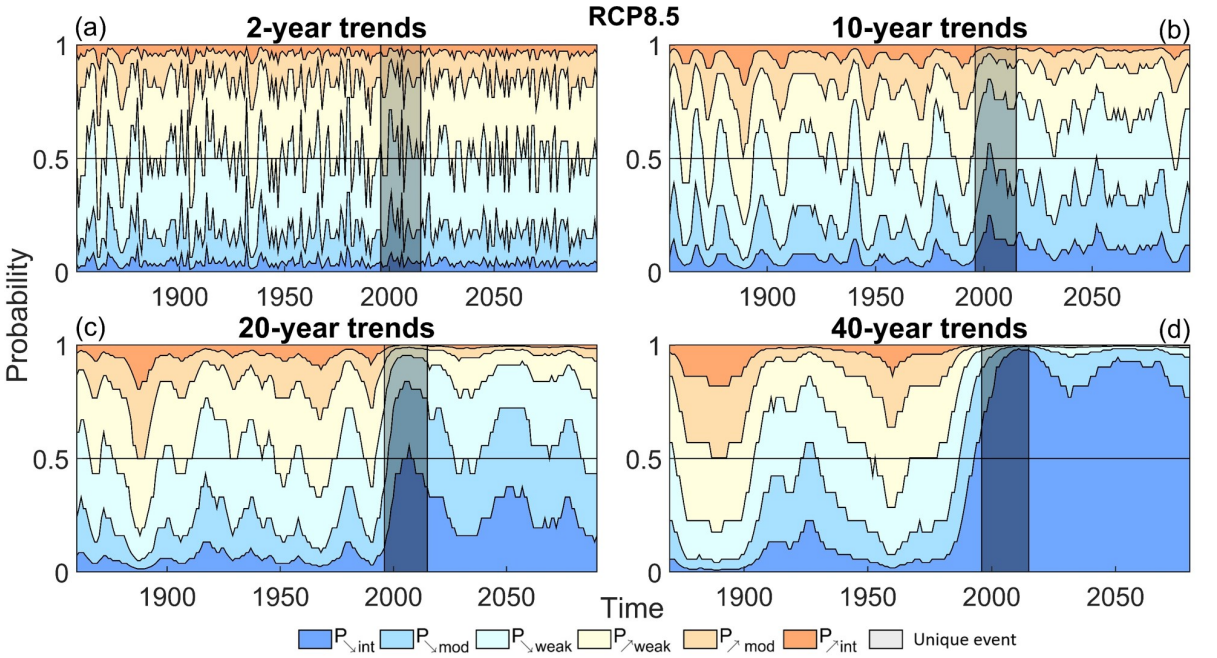

Fig. 4 As Figure 3 but for RCP8.5

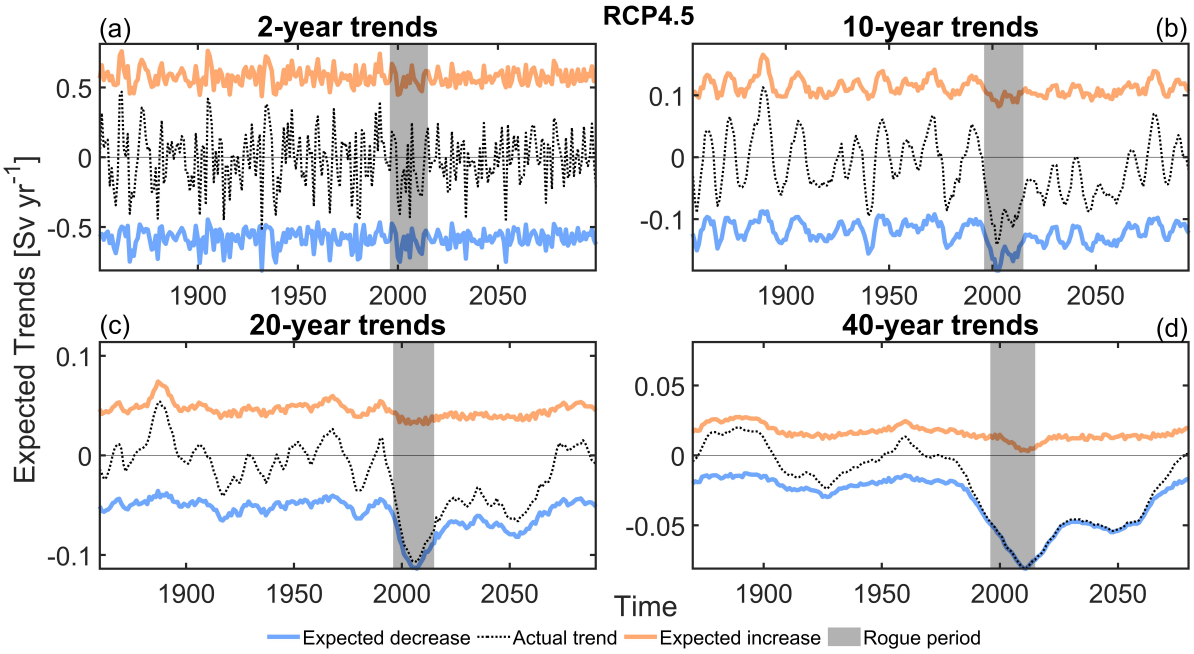

Fig. 5 Actual and expected trends over the historical and future RCP4.5 periods. The time-varying actual (black dotted lines) and expected forced ensemble-mean trend increase (orange lines) and decrease (blue lines) intensities [Sv yr^{-1}] of the AMOC at 48° N from 1850 to 2099 are displayed. The forced trends are filtered over different trend durations: (a) 2 years, (b) 10 years, (c) 20 years, and (d) 40 years. The 20-year unique event from 1995 to 2015 is centred around the 20-year maximum AMOC decline (from subplot c), and shown in grey on all plots

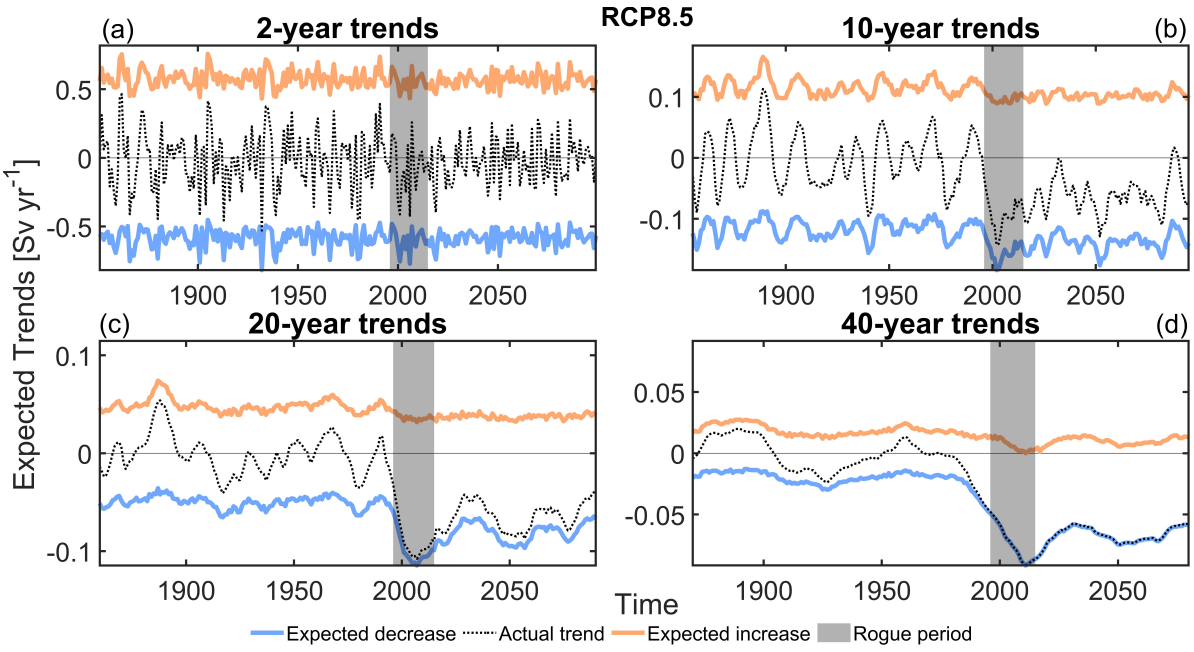

Fig. 6 As Figure 5 but for RCP8.5

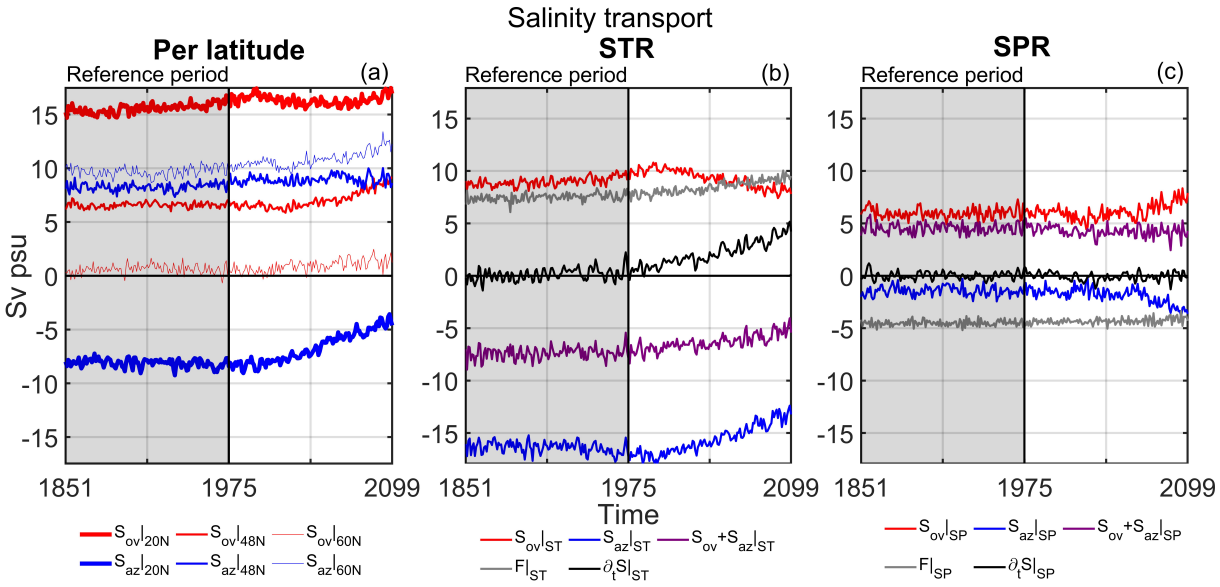

Fig. 7 Annual mean salinity transport [Sv psu] derived from CMIP5 ensemble mean (i.e. forced component) historical and RCP8.5 output from 1851 to 2099. The reference period (1851 to 1975), representing the fluxes almost in equilibrium, is shaded in grey and summarised in the schematic in Figure 8 below. (a) The two oceanic salinity transports: overturning, $\mathscr{S}_{\rm ov}$ (red lines) and horizontal gyre, $\mathscr{S}_{\rm az}$ (blue lines) at the three latitudes marking the meridional boundaries for the subtropical region (STR) and subpolar region (SPR), at 20° N (thick, solid lines), 48° N (weakly thick, solid lines) and 60° N (thin, solid lines). Positive (negative) values indicate northward (southward) fluxes. (b) The STR oceanic salinity transports via $\mathscr{S}_{\rm ov}|_{\rm ST}$ (red line), i.e.,$\mathscr{S}_{\rm ov}|_{20N} - \mathscr{S}_{\rm ov}|_{48N}$ from (a), and $\mathscr{S}_{\rm az}|_{\rm ST}$ (blue line), i.e.,$\mathscr{S}_{\rm az}|_{20N} - \mathscr{S}_{\rm az}|_{48N}$, the combined $\mathscr{S}_{\rm ov} + \mathscr{S}_{\rm az}|_{\rm ST}$ (purple line), the residual (grey line), $\mathscr{F}$, and the total net salinity transports (black line), $\partial_t {\rm S}|_{\rm ST}$, are displayed. (c) SPR transports as in (b), with the southern boundary being 48° N and northern boundary 60° N. Positive (negative) values in (b) and (c) indicate an addition (dilution) of salt in the region

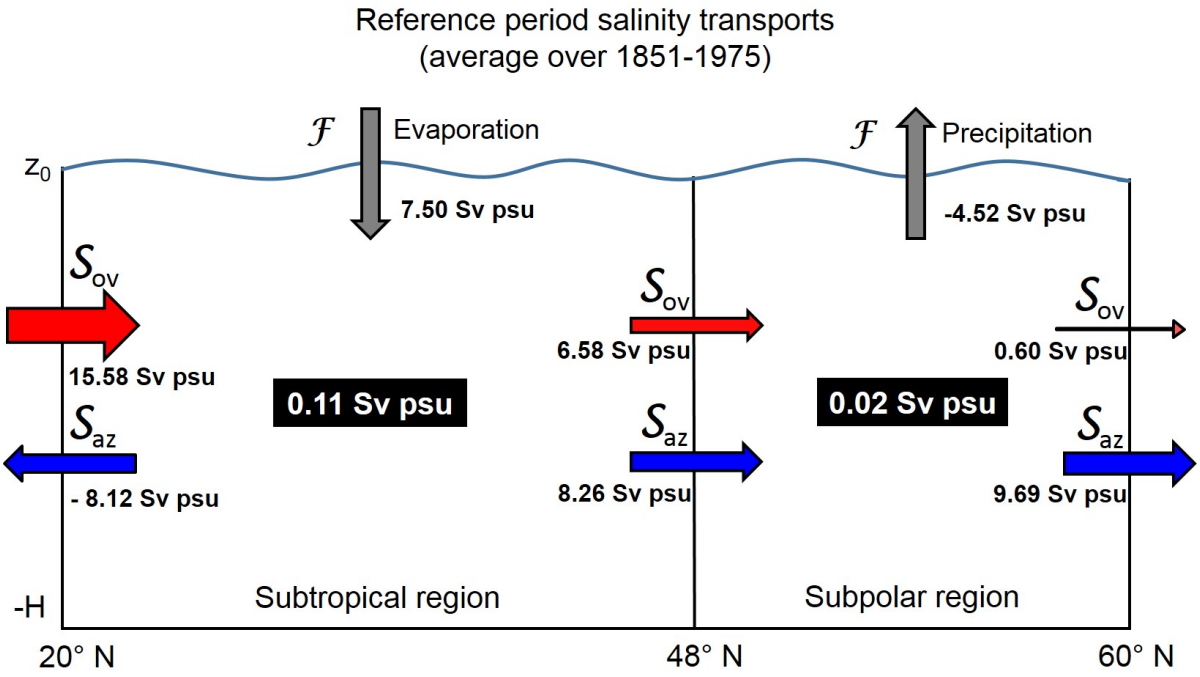

Fig. 8 A schematic displaying the (almost equilibrium) reference period of salinity influx and outflux, temporally averaged over the reference period (1851 to 1975) of the ensemble mean (i.e., forced component), into and out of the subtropical and subpolar regions. The zonally and vertically-integrated oceanic transports comprise of $\mathscr{S}_{ov}$, transport via the overturning component (red arrows), and $\mathscr{S}_{az}$, transport via the azonal, gyre transport (blue arrows). Positive (negative) values indicate northward (southward) fluxes across these latitudes (where all are positive apart from $\mathscr{S}_{az}|_{20N}$). The residual (grey arrows), assumed here to be the atmospheric forcing, $\mathscr{F}$, is computed per region, with a positive value showing net evaporation (indicated by a downward arrow) and a negative value showing net precipitation (indicated by an upward arrow). The small total net salinity trend in each region is the black box (+0.11 Sv psu and +0.02 Sv psu in the STR and SPR, respectively). The width of the arrows are scaled to their strength of transport but the size of the regions is not proportional to the actual size

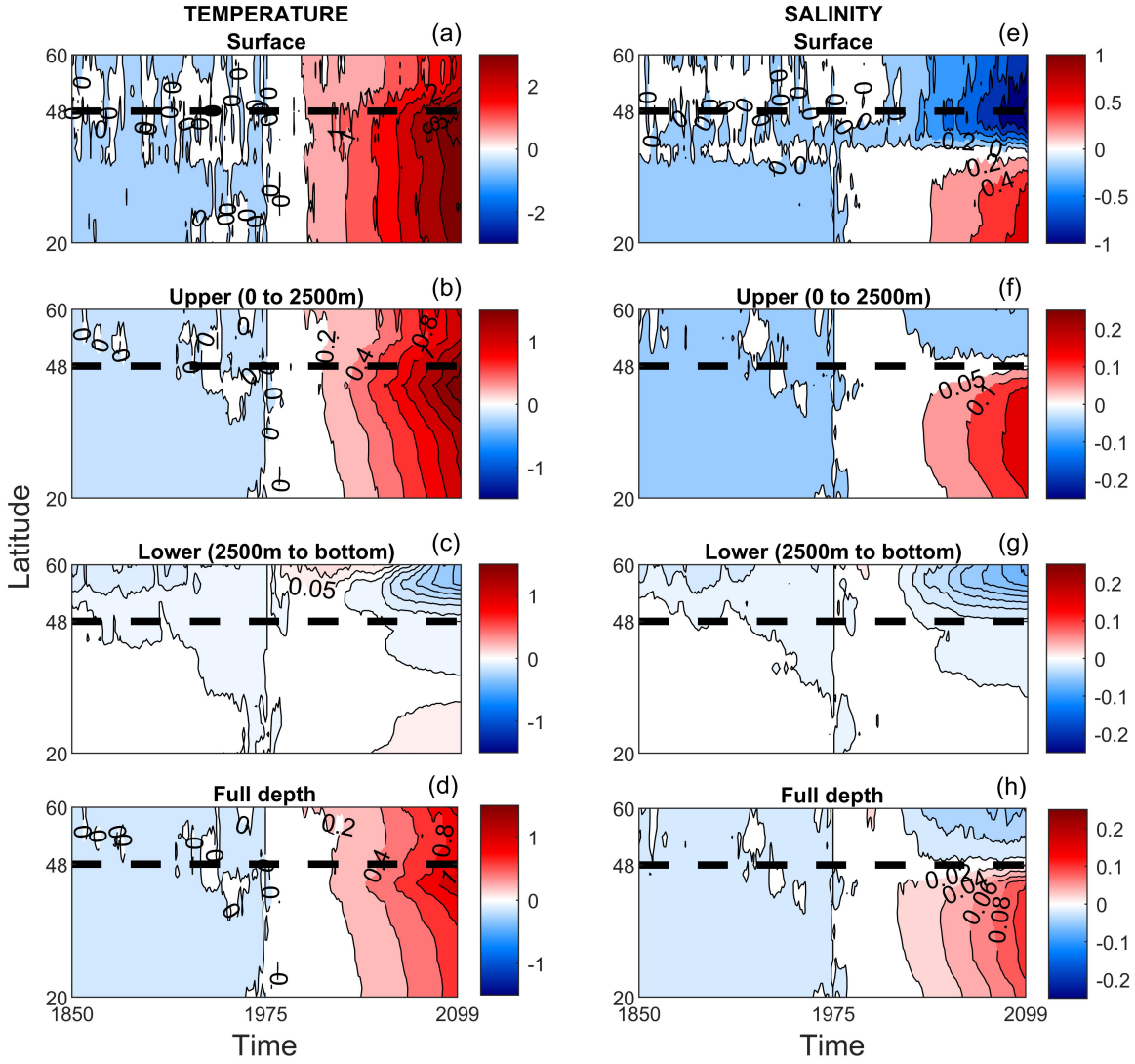

Fig. 9 Hovmöller plots showing zonally and depth average of the forced temperature [K] and salinity [psu] anomalies referenced to 1975 (vertical, black line), from 1850 to 2099 and filtered using 10-year moving means under the RCP8.5 scenario. Displayed as a function of latitude, the boundary between the SPR and STR is shown at 48°N (dashed horizontal, black line). The anomalies are integrated vertically and presented at different depths; at the surface in (a) for temperature and (e) for salinity, averaged over the upper ocean (from 0 to 2,500 m) in (b) for temperature and (f) for salinity, averaged over the lower ocean (from 2,500 m to the bottom) in (c) for temperature and (g) for salinity, and averaged over the full depth in (d) for temperature and (h) for salinity

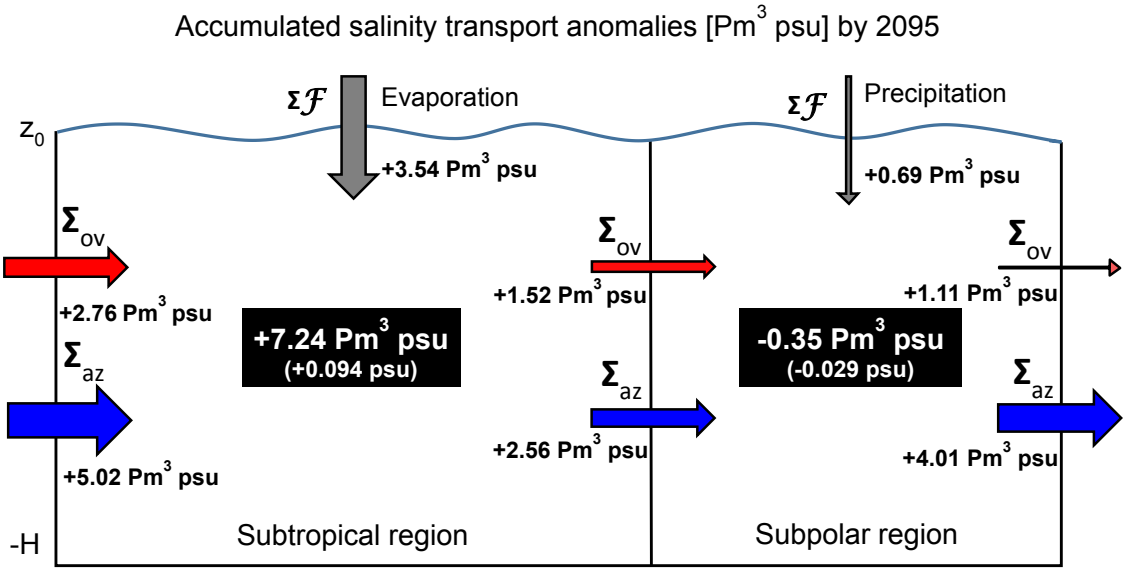

Fig. 10 Schematic of the accumulated forced salinity anomaly transport ($\Sigma\mathscr{S}$) by 2095 referenced to 1975. The direction of the arrows shows whether the accumulated anomaly causes a flux of salinity into or out of the STR and SPR. The equivalent average change in salinity concentration is shown in brackets in the black box for each region (+0.09 psu and −0.03 psu in the STR and SPR, respectively). All other arrows and colours represent the same fluxes as in Figure 8, but are now accumulated transports

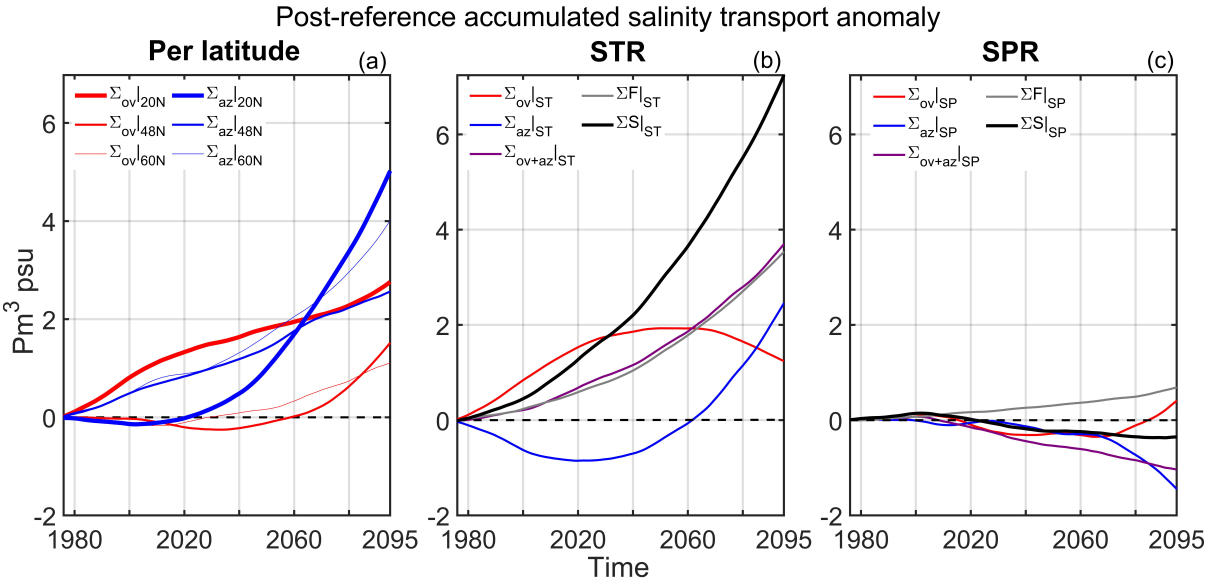

Fig. 11 Accumulated anomalies of forced salinity transport (Σ) from 1975 to 2095, derived from CMIP5 ensemble historical and RCP8.5 data, referenced to the t_{ref} (1975) values, filtered using a 10-year moving average from annually averaged data. Accumulated transport units are in Pm^3 psu (1 $Pm^3 = 10^{15}$ m^3). See Figure 7 for a description of the legend colours

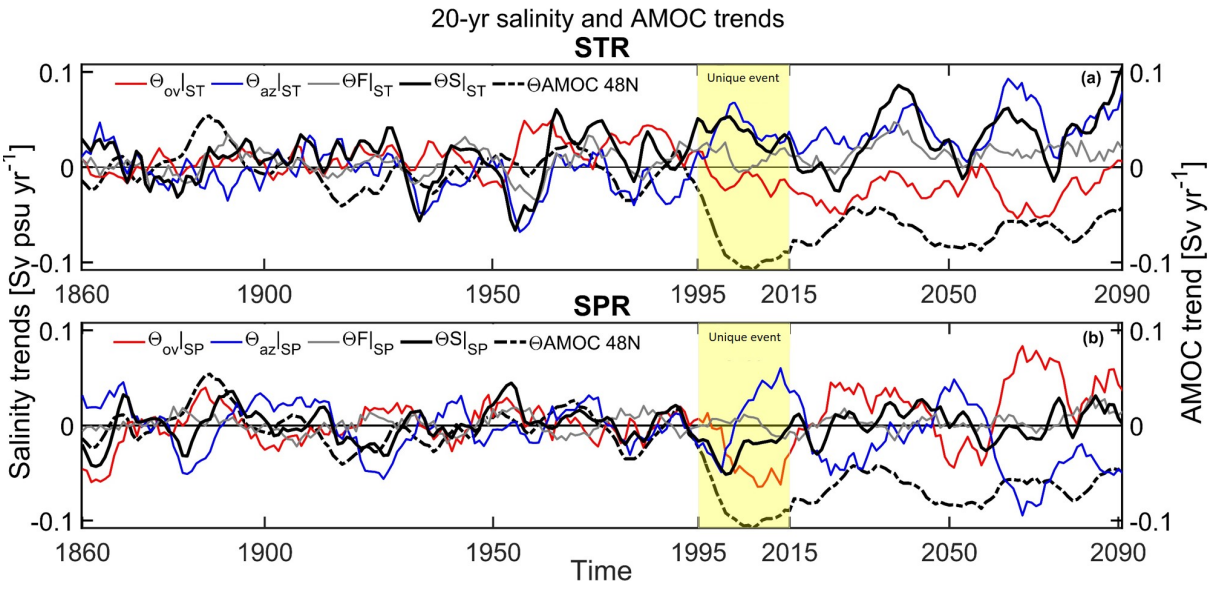

Fig. 12 A comparison of forced salinity and AMOC transport trends ($\Theta\mathscr{S}$ and ΘAMOC, respectively) filtered using 20-year sliding windows from 1850 to 2099 in the (a) subtropical region (STR), and (b) subpolar region (SPR). Linear regression trends are fitted to the raw salinity transport data (for the STR and SPR data in Figure 7b and c, respectively). Legend colours are the same as in Figure 11b and c. The 20-year sliding window trend of the AMOC at 48°N (black, dash-dotted line) is the same timeseries plotted in Figure S3c. The 'unique event' (highlighted in yellow) from 1995 to 2015 marks the period in which the forced component of the AMOC's 20-year trends rapidly fall out of the range of the historical data and overshoot the range found in the 21st century data and lead to an anomalously high probability of interdecadal AMOC slowdown (Figures 3c and 4c)

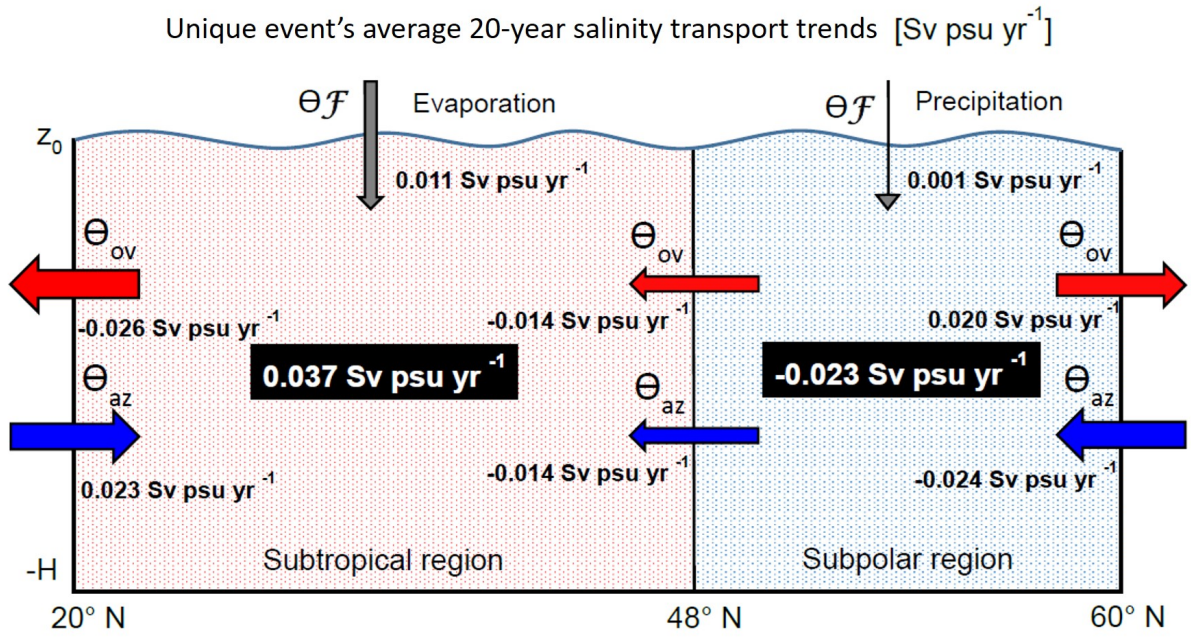

Fig. 13 A schematic of the average 20-year forced salinity transport trends ($\Theta\mathscr{S}$) over the 'unique event' (1995 to 2015, corresponding to the yellow highlighted patch in Figure 12). The arrows therefore now represent trend values, averaged over the unique event, and the colours represent the trends of the fluxes shown in Figure 8

Supplementary Files

This is a list of supplementary files associated with this preprint. Click to download.

- FigS1.jpg
- FigS2.jpg
- supplementaryinfo.pdf